Cambro–Ordovician ferrosilicic magmatism along the northern Gondwana margin: constraints from the Cézarenque–Joyeuse gneiss complex (French Massif Central)

Simon Couzinié, Pierre Bouilhol, Oscar Laurent, Thomas Grocolas, Jean-Marc Montel

BSGF - Earth Sciences Bulletin 2022, 193, 15
© S. Couzinié *et al.*, Published by EDP Sciences 2022
https://doi.org/10.1051/bsgf/2022010

BSGF Earth Sciences Bulletin
Available online at:
www.bsgf.fr

Cambro–Ordovician ferrosilicic magmatism along the northern Gondwana margin: constraints from the Cézarenque–Joyeuse gneiss complex (French Massif Central)

Simon Couzinié[1,*], Pierre Bouilhol[1], Oscar Laurent[2,3], Thomas Grocolas[1,a] and Jean-Marc Montel[1]

[1] Université de Lorraine, CNRS, CRPG, F-54000 Nancy, France
[2] ETH Zürich, Department Erdwissenschaften, Institute for Geochemistry and Petrology, Clausiusstrasse 25, CH-8092 Zürich, Switzerland
[3] CNRS, Observatoire Midi-Pyrénées, Géosciences Environnement Toulouse, 14 avenue E. Belin, F-31400 Toulouse, France

Received: 25 August 2021 / Accepted: 3 June 2022 / Published online: 30 August 2022

Abstract – It is well-acknowledged that the northern margin of the Gondwana supercontinent was affected by a major magmatic event at late Cambrian (Furongian) to early Ordovician (Tremadocian–Floian) times. However, an accurate assessment of its extent, origin, and significance is partly hampered by the incomplete characterization of the numerous gneiss massifs exposed in the inner part of the Variscan belt, as some of them possibly represent dismembered and deformed Furongian–Lower Ordovician igneous bodies. In this study, we document the case of the "Cézarenque–Joyeuse" gneiss complex in the Cévennes parautochthon domain of the French Massif Central. The gneisses form decametre- to kilometre-thick concordant massifs interlayered within a pluri-kilometric sequence of mica- and quartz schists. They encompass two main petrological types: augen gneisses and albite gneisses, both typified by their blue and engulfed quartz grains with the augen facies differing by the presence of centimetre-sized pseudomorphs after K-feldspar and the local preservation of igneous textures. Whole-rock geochemistry highlights that many gneisses have magmatic *ferrosilicic* (acidic with anomalously high FeO_t and low CaO) compositions while others are akin to greywackes. Collectively, it is inferred that the bulk of the Cézarenque–Joyeuse gneisses represents former rhyodacite lava flows or ignimbrites and associated epiclastic tuffs. Volumetrically subordinate, finer grained, and strongly silicic leucogneisses are interpreted as microgranite dykes originally intrusive within the volcanic edifices. LA–ICP–MS U–Pb dating of magmatic zircon grains extracted from an augen gneiss and a leucogneiss brackets the crystallization age of the silicic magmas between 486.1 ± 5.5 Ma and 483.0 ± 5.5 Ma which unambiguously ties the Cézarenque–Joyeuse gneisses to the Furongian–Lower Ordovician volcanic belt of SW Europe. Inherited zircon date distributions, Ti-in-zircon and zircon saturation thermometry demonstrate that they formed by melting at 750–820 °C of Ediacaran sediments. Zircon Eu/Eu* and Ce/Ce* systematics indicate that the melts were strongly reduced (fO_2 probably close to the values expected for the iron–wüstite buffer), possibly because they interacted during ascent with Lower Cambrian black shales. This would have enhanced Fe solubility in the melt phase and may explain the peculiar *ferrosilicic* signature displayed by many Furongian–Lower Ordovician igneous rocks in the northern Gondwana realm. We infer that crustal melting resulted from a combination of mantle-derived magma underplating in an intracontinental rift setting and anomalously elevated radiogenic heat production within the Ediacaran sedimentary sequences.

Keywords: northern Gondwana margin / Furongian–Lower Ordovician volcanic belt / Cambro–Ordovician / French Massif Central / ferrosilicic magmatism / crustal melting

Résumé – Le magmatisme ferrosiliceux cambro–ordovicien de la marge Nord du Gondwana : nouvelles contraintes issues de l'étude du complexe gneissique de la Cézarenque–Joyeuse (Massif Central français). Un important évènement magmatique a affecté la marge Nord du Gondwana de la fin du Cambrien (Furongien) au début de l'Ordovicien (Trémadocien–Floien). Afin de préciser son extension

*Corresponding author: simon.couzinie@univ-lorraine.fr
[a]Present address: Institute of Earth Sciences, University of Lausanne, Géopolis, CH-1015 Lausanne, Switzerland.

géographique et de mieux contraindre son origine et sa signification géodynamique, il est essentiel de caractériser finement les nombreux massifs de gneiss affleurant dans les zones internes de la chaîne Varisque, certains d'entre eux représentant probablement d'anciens corps magmatiques cambro-ordoviciens. Cet article présente de nouvelles données sur les gneiss dits de la « Cézarenque » ou de « Joyeuse » qui affleurent dans le domaine para-autochtone cévenol du sud du Massif Central français. Ces gneiss forment des massifs concordants dans la schistosité régionale, d'une épaisseur variant de la dizaine de mètres à plusieurs kilomètres, intercalés dans une épaisse séquence de mica- et quartz-schistes. Les deux types pétrographiques principaux sont un gneiss oeillé et un gneiss albitique, tous deux caractérisés par la présence de « phénocristaux » de quartz bleus d'origine magmatique, les gneiss oeillés se distinguant par leurs pseudomorphes centimétriques de feldspath potassique. Les compositions chimiques en roche totale démontrent que de nombreux gneiss ont des compositions magmatiques et se rattachent aux séries ferrosiliceuses (acides, anormalement riches en FeO_t et pauvres en CaO). *A contrario*, certains gneiss albitiques ont des compositions qui les rapprochent de grauwackes. L'ensemble de ces observations suggère que les gneiss de Cézarenque–Joyeuse représentent d'anciennes coulées (pyroclastiques ou laviques) rhyodacitiques et leurs produits de remaniements proximaux. Un rare faciès de leucogneiss, subordonné en volume, correspondrait à d'anciens microgranites originellement intrusifs dans les édifices rhyodacitiques. Les datations U–Pb par LA–ICP–MS de grains de zircons extraits d'un gneiss oeillé et d'un leucogneiss indiquent que les magmas ont cristallisé entre 486,1 ± 5,5 et 483,0 ± 5,5 Ma, affiliant de fait les gneiss de Joyeuse–Cézarenque à la chaîne volcanique d'âge Furongien–Ordovicien Inférieur d'Europe de l'Ouest. La gamme d'âge des zircons hérités et la teneur en Ti des zircons magmatiques indiquent que les liquides proviennent de la fusion à 750–820 °C de sédiments d'âge Ediacarien. Les ratios Eu/Eu* et Ce/Ce* des grains de zircon démontrent que ces liquides étaient fortement réduits (fO_2 proche du tampon fer–wustite), potentiellement à la suite de leur interaction en route vers la surface avec les sédiments riches en matière organique du Cambrien Inférieur. Ce caractère réduit a pu augmenter la solubilité du fer dans les liquides et expliquerait de fait le caractère ferrosiliceux. Cet évènement de fusion partielle de la croûte continentale est vraisemblablement lié au sous-placage de magmas basiques dans un contexte de rift intracontinental et à la production de chaleur radiogénique anormalement élevée des séquences sédimentaires édiacariennes.

Mots clés : marge nord-gondwanienne / chaîne volcanique d'âge Furongien–Ordovicien Inférieur / Cambro–Ordovicien / Massif Central français / magmatisme ferrosiliceux / fusion de la croûte continentale

1 Introduction

The basement of southwestern Europe consists of Gondwana-derived crustal blocks amalgamated during the Devonian–Carboniferous Variscan orogeny (*e.g.*, Kroner and Romer, 2013; and references therein). A wealth of studies have documented the common occurrence within the Variscan metamorphic series of late Cambrian to early Ordovician (Furongian–Tremadocian–Floian: ~497–470.0 ± 1.4 Ma, Cohen *et al.*, 2013) felsic (meta) igneous rocks (Parga Pondal *et al.*, 1964; Weisbrod and Marignac, 1968; Weisbrod, 1969; Guérangé-Lozes and Burg, 1990; Bea *et al.*, 2007; Montero *et al.*, 2007; Díez Montes *et al.*, 2010; Melleton *et al.*, 2010; Ballèvre *et al.*, 2012; Díez Fernández *et al.*, 2012; Talavera *et al.*, 2013; Lopez-Sanchez *et al.*, 2015; Gutiérrez-Alonso *et al.*, 2016; Pouclet *et al.*, 2017; Álvaro *et al.*, 2020), the largest and most iconic example being the Ollo de Sapo formation in the Iberian Massif (see review in García-Arias *et al.*, 2018). Considered together, the Furongian–Lower Ordovician igneous rocks delineate a > 2000 km-long arcuate volcanic-plutonic belt (Fig. 1) and shed light on a major magmatic event at the northern Gondwana margin by that time.

Unravelling the spatial extent, duration, origin, and magma volumes emitted during this event is of marked importance since it has recently been suggested that the Furongian–Lower Ordovician belt would classify as a silicic Large Igneous Province (Díez Montes *et al.*, 2010; Gutiérrez-Alonso *et al.*, 2016; García-Arias *et al.*, 2018) and hence would have had a strong influence on the early Ordovician climate and the living (Bryan, 2021). Besides, the acidic magmas (SiO_2: 65–70 wt.%) emitted during this magmatic flare-up have unusual compositions termed *ferrosilicic* (Fernández *et al.*, 2008; Castro *et al.*, 2009) as they show anomalously high FeO_t (> 2.5 wt.%) and low CaO (< 2.0 wt.%) contents. Even though melting of pre-existing crustal materials is generally advocated (Bea *et al.*, 2007; Ballèvre *et al.*, 2012; Montero *et al.*, 2017), the origin of this peculiar signature remains debated (Castro *et al.*, 2009; Díaz-Alvarado *et al.*, 2016; Fiannacca *et al.*, 2019). Finally, it is well-established that this magmatic event is coeval to the opening of the Rheic ocean (Murphy *et al.*, 2008; Nance *et al.*, 2010), yet, the actual trigger of crustal melting is disputed with models invoking extensional (Bea *et al.*, 2007; Ballèvre *et al.*, 2012; Pouclet *et al.*, 2017; Álvaro *et al.*, 2020) or contractional (Villaseca *et al.*, 2016) settings, near or far from the influence of a waning Cadomian subduction zone (Fernández *et al.*, 2008; Castro *et al.*, 2009; Villaseca *et al.*, 2016).

This study focuses on the so-called Cézarenque–Joyeuse gneiss complex exposed in the Cévennes domain of the southeastern French Massif Central (Fig. 1). Ballèvre *et al.* (2012) postulated that they could represent felsic igneous rocks of the Furongian–Lower Ordovician belt having experienced greenschist- to lower amphibolite-facies metamorphism during the Variscan orogeny. We explore this possibility by reviewing the field relationships, petrography and geochemistry of these gneisses and providing the first LA–ICP–MS zircon U–Pb and trace element data on such lithologies.

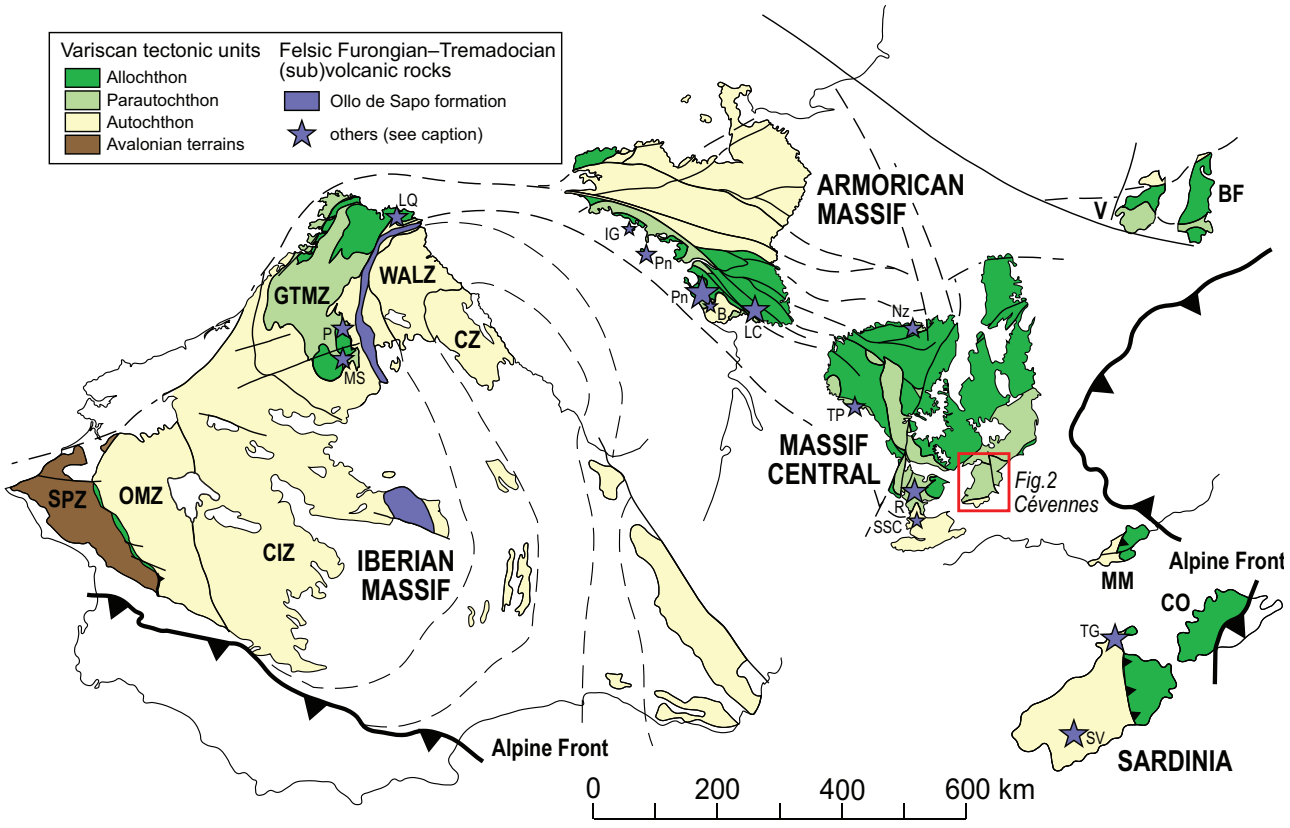

Fig. 1. Sketch map of the Variscan terrains of SW Europe outlining the location of several felsic (sub)volcanic complexes of Furongian–Lower Ordovician age, adapted from Ballèvre *et al.* (2014). Zones in the Iberian Massif: CIZ: Central Iberian; CZ: Cantabrian; GTMZ: Galicia–Trás-os-Montes; OMZ: Ossa-Morena; SPZ: South-Portuguese; WALZ: West Asturian–Leonese. V: Vosges; BF: Black Forest; MM: Maures Massif; CO: Corsica. Abbreviations for the (sub)volcanic formations. In the Iberian Massif, LQ: Loiba and Queiroga series (Valverde-Vaquero *et al.*, 2005); MS: Mora and Saldanha volcanic complexes (Dias Da Silva *et al.*, 2014); P: volcanics from the Paraño Group in the Bragança–Alcañices area (Farias *et al.*, 2014). Armorican Massif, Pn: Porphyroid nappe and B: Brétignolles metavolcanics (Ballèvre *et al.*, 2012); IG: Île-de-Groix felsic gneisses (El Korh *et al.*, 2012); LC: La Châtaigneraie metavolcanics (Bouton and Branger, 2008). In the Massif Central, the Larroque rhyolitic formation in the St-Sernin-sur-Rance (R) and St-Salvi-de-Carcavès nappes (SSC) (Guérangé-Lozes and Burg, 1990; Pouclet *et al.*, 2017); TP: the Génis rhyolites in the Thiviers-Payzac Unit (Melleton *et al.*, 2010; Pouclet *et al.*, 2017); Nz: the Nouzier metavolcanics (Quesnel *et al.*, 2009). In Sardinia, SV: San Vito Formation volcanites and TG: Li Trumbetti and Mt. Geisgia rhyolites (Oggiano *et al.*, 2010).

Collectively, our results do tie the Cézarenque gneisses to the Furongian–Lower Ordovician magmatic event, provide novel constraints on the petrogenesis of ferrosilicic magmas and offer the opportunity to address the tectonic evolution of this segment of the northern Gondwana margin.

2 Geological setting

The French Massif Central (FMC) is built up by igneous and metamorphic rocks formed during the Variscan orogeny (Matte, 2007; Faure *et al.*, 2009a) which itself resulted from the closure of one or several oceanic domains in the early Devonian followed by the late Devonian to Carboniferous collision of Gondwana, Laurussia and several microblocks (Vanderhaeghe *et al.*, 2020, and references therein). At the scale of the eastern Massif Central, several tectonic–metamorphic nappes were identified (Burg and Matte, 1978; Ledru *et al.*, 1989; Faure *et al.*, 2009a), all of which being exposed in the Cévennes area. At the top, the Upper Gneiss Unit experienced a Devonian (c. 380–360 Ma, Chelle-Michou *et al.*, 2017; Lotout *et al.*, 2020, 2018) prograde high-pressure metamorphism, with peak conditions of ~800 °C and 10–14 kbar at Marvejols (Fig. 2, Bodinier *et al.*, 1988). During its retrograde evolution, it was thrust at 360–340 Ma (Chelle-Michou *et al.*, 2017; Costa, 1989) over a set of nappes devoid of HP record (and experiencing prograde metamorphism) which were locally subdivided into a Lower Gneiss Unit and a Parautochthonous Unit (Faure *et al.*, 2009a). Those experienced a pervasive and protracted melting episode at 335–300 Ma as a result of crust thickening and marked heat advection from the mantle (Laurent *et al.*, 2017). At the bottom of the nappe pile lays the barely metamorphic "Fold-and-Thrust Belt" (Faure *et al.*, 2009a), which corresponds to the so-called "Viganais series" in the Cévennes area (Fig. 2). The whole sequence was unconformably overlain by Upper Carboniferous to Lower Permian coal-bearing sedimentary rocks.

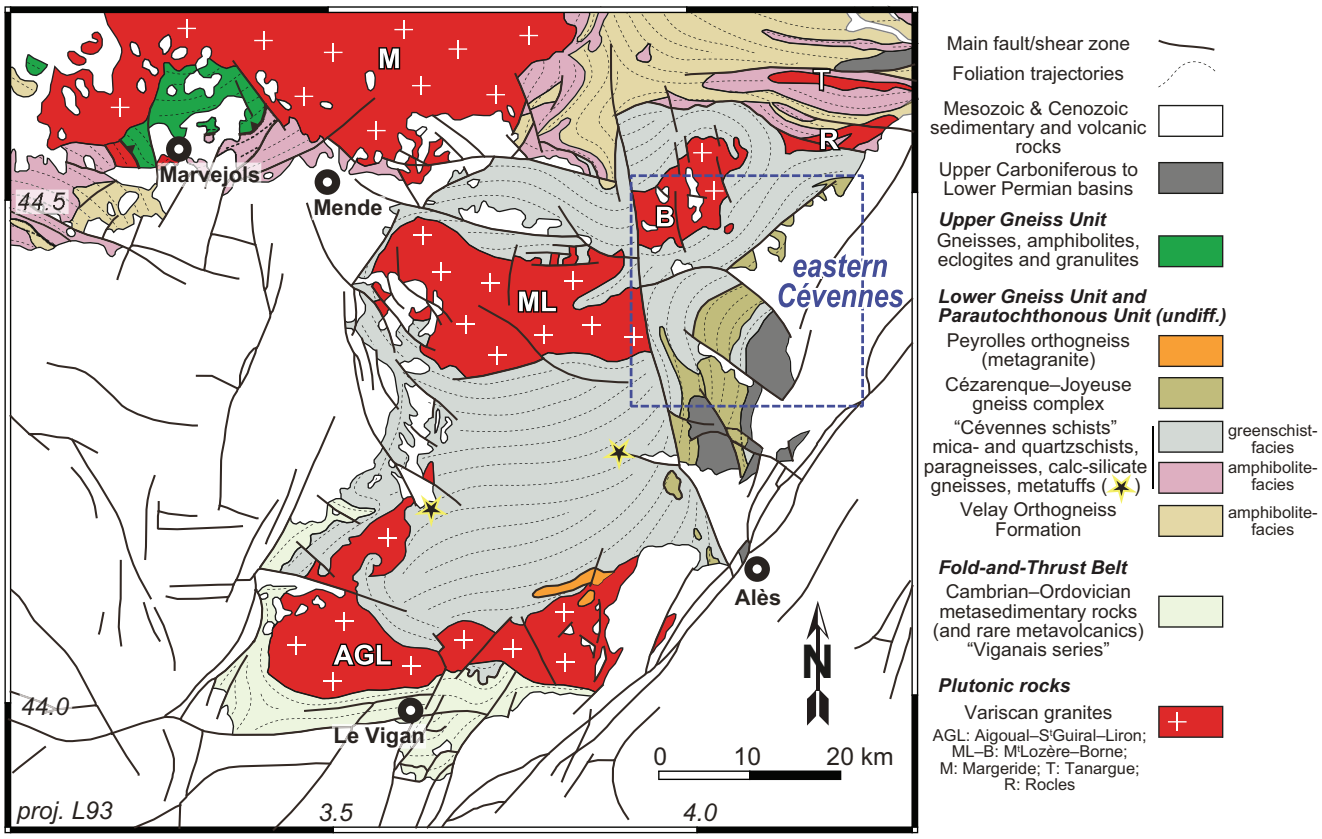

Fig. 2. Geological map of the Cévennes domain outlining the main lithotectonic formations. Redrawn and adapted from Chantraine *et al.* (2003).

2.1 Tectonic-metamorphic evolution of the Cévennes domain

The Cévennes domain is primarily composed of detrital metasediments including a wide variety of petrographic types (mica and quartz schists, locally feldspar-rich, quartzite, calc-silicate gneisses, paragneisses) commonly gathered under the term "Cévennes schists" (Brouder, 1963; Barbey *et al.*, 2015). It also encompasses several gneiss massifs (Peyrolles, Cézarenque–Joyeuse, Fig. 3), all of which forming decametre- to (several) kilometre-thick concordant bodies within schists (Brouder, 1963; Weisbrod and Marignac, 1968; Roger, 1969). At the regional scale, four main tectonic-metamorphic events were described. The main deformation phase D_1 produced a near-horizontal schistosity S_1 with a N–S stretching and mineral lineation, a fabric resulting from a combination of pure and simple shear with top-to-the S kinematics (Mattauer and Etchecopar, 1976; Lacassin and van den Driessche, 1983). Ar–Ar dating of micas and amphibole yielded 340–330 Ma dates for D_1 (Caron, 1994) which took place under metamorphic conditions of c. 500 °C and 5.2 kbar (Arnaud, 1997) and would attest to an early crust thickening and nappe stacking stage (Toteu and Macaudière, 1984; Faure *et al.*, 2009b). In the eastern Cévennes, Faure *et al.* (2009b) advocated that the Cézarenque–Joyeuse gneisses and overlying micaschists represent an allochthonous complex (klippen) stacked over schists during D_1, putting forward the existence of a high-strain zone at the base of the main gneiss massif (Mattauer and Etchecopar, 1976). This complex was thus regarded as an equivalent of the Lower Gneiss Unit, and the underlying schists attributed to the Parautochthonous Unit sensu Faure *et al.* (2009a). Alternative views consider that all metamorphic rocks from the Cévennes (including the Cézarenque–Joyeuse gneisses) belong to the Parautochthonous Unit (Matte, 2007).

A D_2 event affecting the Cézarenque–Joyeuse gneisses and abutting schists was identified by Bouilhol *et al.* (2006). It is typified by asymmetric folding reworking S_1, a NW–SE trending stretching lineation and local C/S structures collectively indicating top-to-the NW displacements. The P–T conditions of this event are ill-defined. The D_3 event took place in the time period 320–310 Ma (Caron, 1994; Couzinié *et al.*, 2021) while a thermal anomaly developed beneath the Cévennes and resulted in a LP–HT metamorphic field gradient (Chenevoy and Ravier, 1968; Weisbrod, 1968; Tobschall, 1971; Montel *et al.*, 1992; Rakib, 1996; Bouilhol *et al.*, 2006) with peak temperatures reaching 700–800 °C at 3–6 kbar in the southern Velay dome (Ledru *et al.*, 2001; Barbey *et al.*, 2015; Villaros *et al.*, 2018; Couzinié *et al.*, 2021). Evidence for top-to-the-NE shearing during D_3 are conspicuous in the northern Cévennes (Faure *et al.*, 2001; Bouilhol *et al.*, 2006). The D_4 event (310–295 Ma) features the widespread crystallization of retrograde, greenschist-facies mineral assemblages associated with (brittle-)ductile top-to-the-ESE shearing (Faure *et al.*, 2001) and the emplacement of the main granite plutons of the Cévennes (Borne, Mont-Lozère, Aigoual–St-Guiral–Liron; Brichau *et al.*, 2007; Couzinié *et al.*, 2014; Laurent *et al.*, 2017). This event

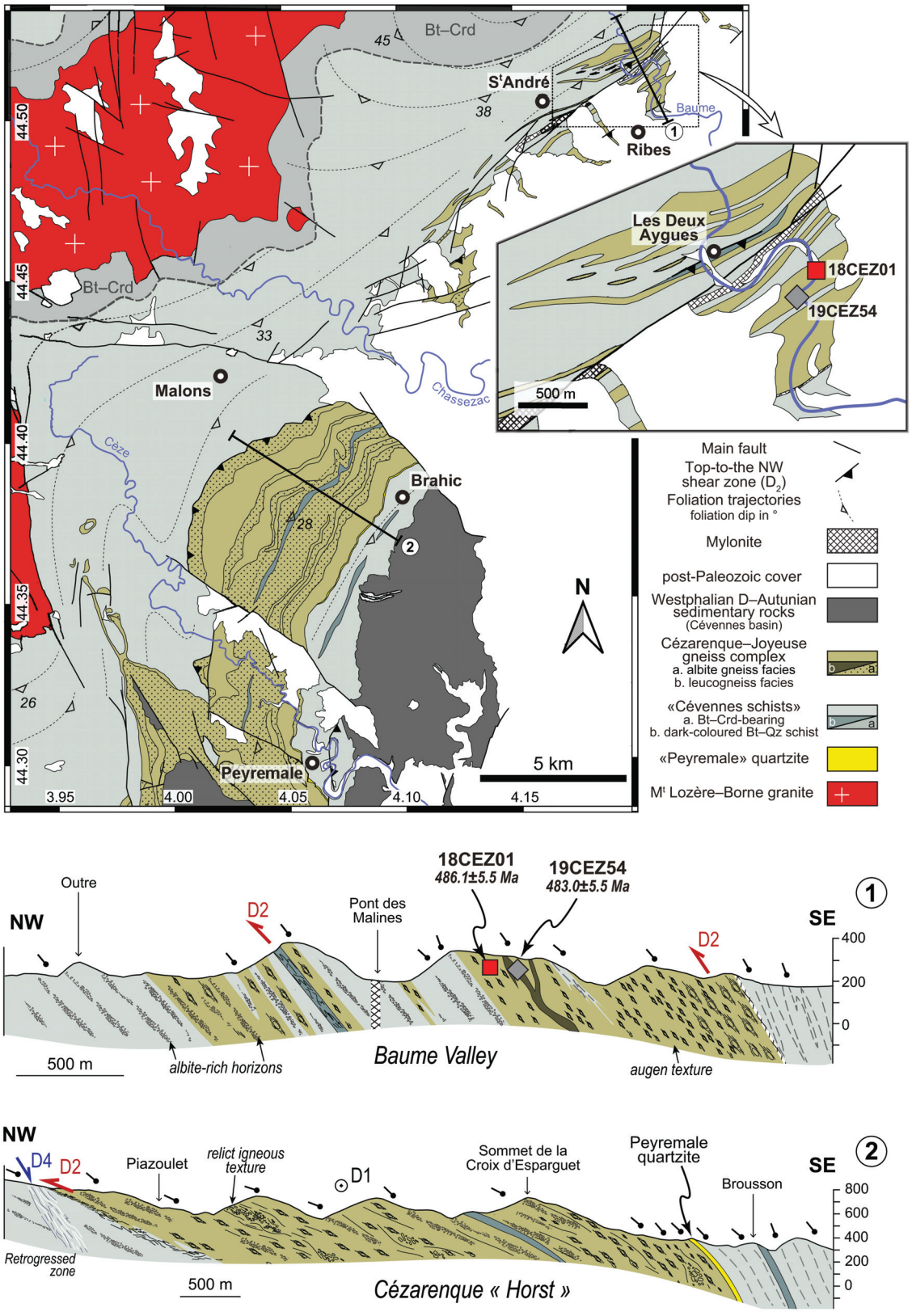

Fig. 3. Geological map and associated interpretative cross-sections of the eastern Cévennes highlighting the intricate association between the different gneiss facies and the "Cévennes schists". The location of the dated samples is indicated in the inset and the cross-section centred on the Baume valley. Map redrawn and adapted from the works of Elmi *et al.* (1974, 1989) and Bouilhol *et al.* (2006).

stamps the transition to an extensional regime which led to the opening of the Alès (Westphalian D–Autunian) coal basin (Allemand *et al.*, 1997).

2.2 Nature and age of the metamorphic protoliths

In the northern Cévennes, where the deepest structural levels are exposed (Faure *et al.*, 2001; Arnaud *et al.*, 2004), amphibolite-facies metasediments yielding Ediacaran zircon U–Pb maximum depositional ages between 592.4 ± 5.5 and 568.3 ± 4.9 Ma (Couzinié *et al.*, 2019) are interlayered with augen gneiss and "leptynites" (a disused term somewhat equivalent to fine-grained leucogneisses) of the Velay Orthogneiss Formation, a former c. 540 Ma-old S-type granitic complex which was originally intrusive within the sedimentary protoliths (Couzinié *et al.*, 2017).

In the central Cévennes, decametric gneiss layers (stars on Fig. 2) within mica and quartz schists, interpreted as felsic metavolcanics, yielded eruption ages of 482 ± 8 and 476 ± 6 Ma (zircon Pb evaporation, Faure *et al.*, 2009b). Further south, the Peyrolles orthogneiss is a metagranite which emplacement age was estimated at 433 ± 4 Ma (zircon U–Pb LA–ICP–MS, Faure *et al.*, 2009b) or 465 ± 12 Ma (Rb–Sr whole-rock isochron; Sabourdy, 1975). Collectively, these data demonstrate that the sedimentary protoliths of the "Cévennes schists" were deposited from the late Ediacaran to the Ordovician.

In the eastern Cévennes (Figs. 2 and 3), the origin of the "Cézarenque–Joyeuse" gneiss complex (Elmi *et al.*, 1974, 1989) is disputed and its age unknown. The gneisses form decametre- to kilometre-thick concordant bodies within mica schists (Brouder, 1963; Weisbrod and Marignac, 1968; Roger, 1969) and were variously interpreted as former volcano (-sedimentary) rocks including felsic lavas and ignimbrites (Chenevoy, 1968a, 1968b; Faure *et al.*, 2001), intrusive granitic bodies (Crevola *et al.*, 1983; Elmi *et al.*, 1989) or detrital sedimentary rocks reworking igneous material (conglomerates, Weisbrod and Marignac, 1968).

3 Lithological components of the eastern Cévennes

3.1 The "Cézarenque–Joyeuse" gneiss complex

Based on available descriptions from the literature (Brouder, 1963; Elmi *et al.*, 1974, 1989; Magontier, 1988) and our own field observations, three lithological facies were identified: augen gneisses, albite gneisses, and leucogneisses. Their descriptions (presented below) are complemented by a review of their whole-rock major element compositions, based on a compilation of available data (Chenevoy, 1968b; Weisbrod, 1970; Magontier, 1988; Elmi *et al.*, 1989) supplemented by two new analyses of an augen gneiss and a tourmaline-bearing leucogneiss (dated samples, see Sect. 4). Their whole-rock chemical compositions were analysed at the Service d'Analyse des Roches et Minéraux (SARM, CNRS, Nancy) from powdered samples using a Thermo Fischer ICap 6500 ICP-OES for major elements and a Thermo Fisher X7 Q-ICP-MS for Zr. The analytical procedures, reproducibility and limits of detection are detailed in Carignan *et al.* (2001). The compilation and the newly obtained data are provided in the Supplementary Table 1.

In the literature, the term "leptynite" was traditionally used to describe any quartz–feldspar rich (and with < 5 vol.% mica) granofelsic to gneissic lithology and thus encompasses both felsic meta-igneous rocks and impure metasandstones and arkoses. Hence, samples referred to as "leptynites" were screened to retain only those of igneous compositions by: (i) a careful examination of the field descriptions (notably evidence for original intrusive relationships) and, (ii) applying the procedure of Davoine (1969), *i.e.*, selecting the high SiO_2 analyses that met the criteria: $(K_2O + Na_2O) > 7\%$ and $CaO < 2\%$. This way, a total of 71 analyses from the previous studies were retained for the three main gneiss facies. In the following, we assume that the whole-rock compositions were not significantly modified during the Variscan metamorphic evolution, as demonstrated for other gneiss massifs of the eastern Massif Central (Couzinié *et al.*, 2017). Geochemical diagrams were plotted using GCDkit (Janoušek *et al.*, 2006).

3.1.1 The augen gneisses

The augen gneisses are strongly to poorly foliated rocks typified by their mm- to cm-sized bluish quartz porphyroclasts generally making up 5–10% of the rock (Figs. 4a–4c). Such grains show undulose extinction and are very commonly "corroded" and engulfed (Fig. 5a). Near rectangular (euhedral) to ovoid (lenticular) 1 to 10 cm-large polycrystalline aggregates (Figs. 4a–4c; 5–20% of the rock) dominantly comprise albite plus quartz and were demonstrated to represent pseudomorphs after K-feldspar (Chenevoy, 1968b), in agreement with the local preservation of microcline in their inner part (Fig. 5b). Bluish quartz and feldspar aggregates are embedded in a fine-grained (av. 0.5 mm) foliated matrix of quartz, albite, muscovite, and biotite (often chloritized). The occurrence of scarce garnet in the matrix along with relictual oligoclase and microcline was reported by Elmi *et al.* (1989). From a chemical point of view, the augen gneisses show elevated SiO_2 (av. ~68.5 wt.%) and FeO_t (av. ~3.9 wt. %), but distinctively low CaO (always < 1.5 wt.%) contents. In the Al/3-Na *vs.* Al/3-K diagram of de La Roche (1968), designed to discriminate igneous and sedimentary rocks, their compositions largely overlap with those of silicic Variscan plutonic and volcanic rocks of similar SiO_2 contents (Fig. 6a) demonstrating that the protoliths of the augen gneisses were igneous rocks. They show subalkaline rhyodacite compositions (Fig. 6b) and are highly peraluminous (Fig. 6c) which, together with the high Fe and low Ca contents, indicates that the igneous protoliths of the augen gneisses share a ferrosilicic signature (in the sense of Castro *et al.*, 2009). Considering the alkalinity and Fe/Mg balance, the augen gneisses classify as calc-alkaline to alkali-calcic and magnesian (both sensu Frost *et al.*, 2001, Figs. 6d and 6e) with $FeO_t/(FeO_t + MgO)$ clustering around 0.7–0.75. Their $K/(K + Na)$ ratios are always close to 1 (Fig. 6f).

3.1.2 The albite gneisses

The albite gneisses (Fig. 4d) are composed of a foliated fine-grained (< 0.2 mm) matrix of quartz, albite, biotite (often chloritized) and muscovite, with some albite porphyroblasts

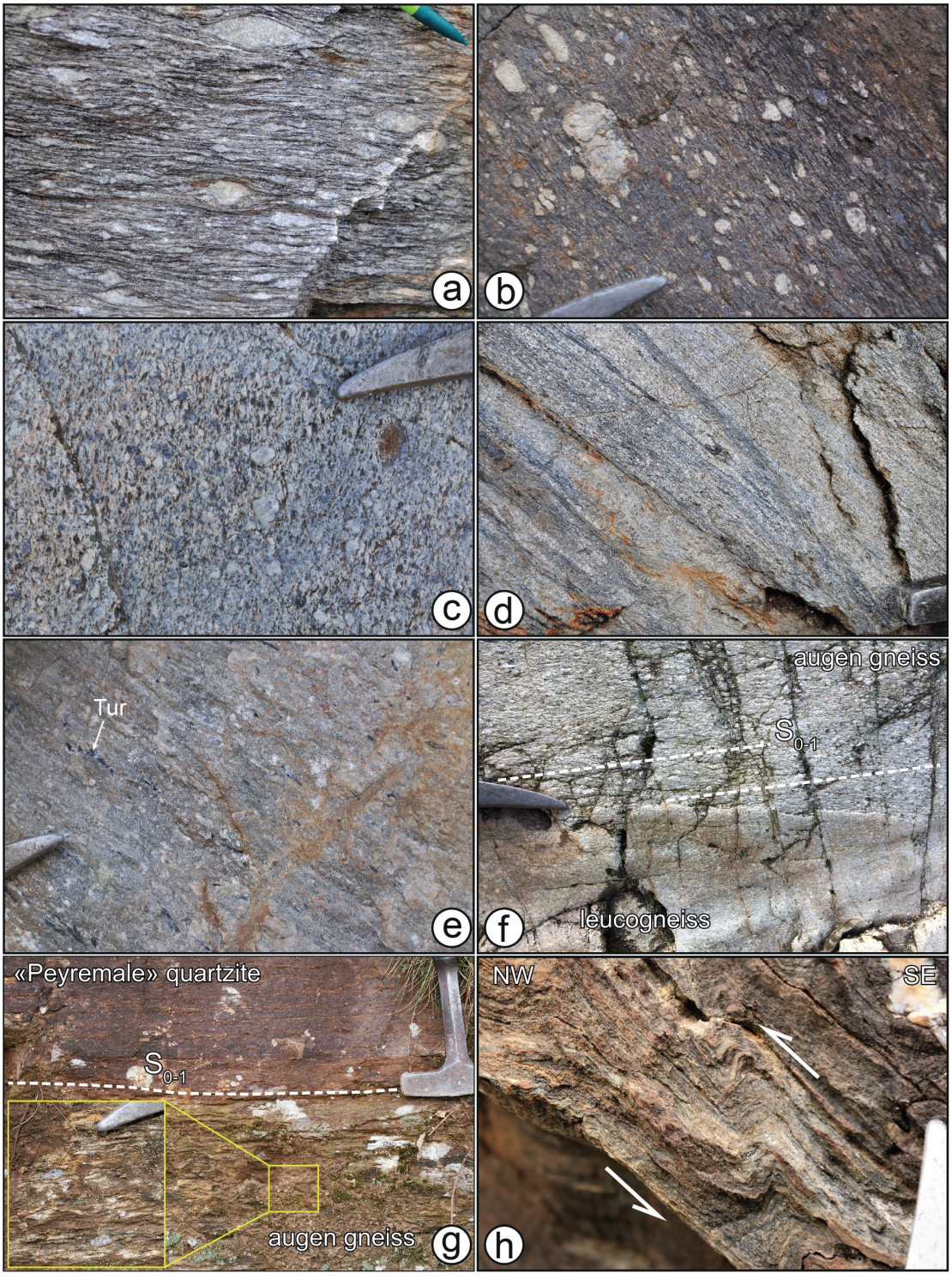

Fig. 4. Representative photographs of the Cézarenque–Joyeuse gneisses and their relationships with adjacent lithologies: (a) augen gneiss with a well-developed foliation, cm-sized lenticular quartz-feldspar aggregates and bluish quartz grains (44.3884°N, 4.0876°E); (b) poorly-foliated augen gneiss facies with euhedral K-feldspar and blue quartz phenocrysts embedded in a finer-grained matrix (44.3935°N, 4.0787°E); (c) augen gneiss, dated sample 18CEZ01 (44.5130°N, 4.2134°E); (d) isoclinally folded albite gneiss (44.5023°N, 4.1224°E); (e) fine-grained tourmaline-bearing leucogneiss, dated sample 19CEZ54 (44.5103°N, 4.2107°E); (f) oblique contact between a leucogneiss and the S_{0-1} foliation of the augen gneiss, interpreted as former intrusive relationships (44.5124°N, 4.2135°E); (g) concordant contact between the S_{0-1} foliation of the augen gneisses and the overlying "Peyremale" quartzite (44.3526°N, 4.0676°E); (h) asymmetric folds in schists, interpreted as evidence for local top-to-the-NW shearing at the gneiss–schist contact (44.4750°N, 4.1309°E).

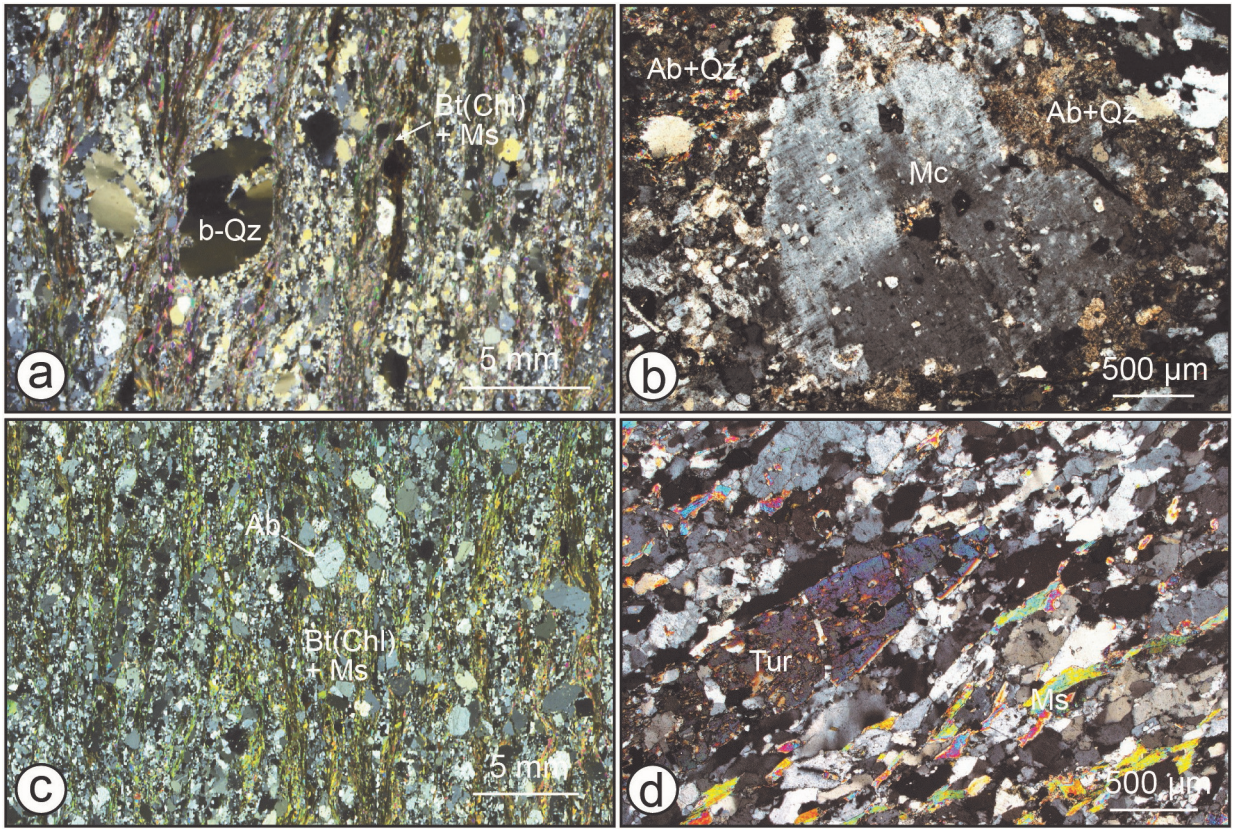

Fig. 5. Representative thin section photomicrographs of the Cézarenque–Joyeuse gneisses: (a) augen gneiss with 0.5 cm-sized engulfed quartz grains embedded in a finer-grained foliated matrix with alternating layers of quartz–albite and biotite (chloritized)–muscovite; (b) close-up on the inner part of a 2 cm-sized lenticular quartz–feldspar aggregate showing the preservation of relict K-feldspar (microcline) surrounded by a fine albite (sericitized)–quartz association; (c) albite gneiss with alternating fine-grained quartz–albite and biotite (chloritized)–muscovite layers overgrown by mm-sized albite porphyroblasts; (d) leucogneiss composed of a foliated quartz, feldspar and muscovite assemblage with truncated tourmaline grains (dated sample 19CEZ54, see text and Fig. 4).

locally reaching 1–2 mm (Fig. 5c). Muscovite and albite are overall more abundant than in the augen facies. Fragments of ovoid strongly stretched (dismantled) feldspar aggregates along with mm-sized bluish quartz grains locally occur in the foliated groundmass but remain scarce and of smaller size than in the augen gneisses. From a chemical point of view, the compositions of albite gneisses are more varied than those of their augen counterparts (*e.g.*, SiO_2: 57–72%). A clear overlap exists as illustrated by most geochemical plots but two thirds of the albite gneisses are typified by higher Al–Fe–Mg (Figs. 6a and 6c) together with lower SiO_2 and alkali contents (Fig. 6b) with respect to the augen facies. Such samples plot in the fields of greywackes (60%) and shales (40%) in the Al/3-Na *vs.* Al/3-K diagram of de La Roche (1968) and their compositions resemble those of the Cévennes mica schists, albeit differing by more elevated alkali ($Na_2O + K_2O$) *vs.* CaO ratios (Fig. 6).

3.1.3 The leucogneisses

The leucogneisses are leucocratic fine-grained (< 0.2 mm) rocks (Figs. 4e and 4f) typified by their foliated (or lineated) "granitic" assemblage of albite (20–25 vol.%), quartz (30–40%) and K-feldspar (microcline, 15–25%) and a lower mica content with respect to other gneiss varieties (< 10–15%), with muscovite always more abundant than biotite (Fig. 5d). Locally, subhedral cm-sized grains of tourmaline, partly corroded, recrystallized, and truncated (Fig. 5d), underline the rock stretching lineation. The leucogneisses are strongly silicic (SiO_2: 72–76 wt.%) and plot in the field of meta-igneous rocks in the diagram of de La Roche (1968). They have rhyolitic compositions (Fig. 6b), are felsic peraluminous, calc-alkaline and slightly potassic (K/Na + K: 0.5–0.6, Figs. 6c–6e) and show variable Fe/Mg ratios (Fig. 6f).

3.2 The "Cévennes schists"

This term encompasses a variety of metamorphic rocks derived from a range of pelite, semi-pelite, greywacke, sandstone, and arkose protoliths. The most representative petrographic type is a mica schist showing a well-developed foliation (Fig. 7a) defined by alternating mm-scale quartz and chlorite–muscovite (± graphite ± biotite ± garnet) layers. The mode of quartz can significantly increase and the rocks grade to quartz schists (Fig. 7b). Albite porphyroblasts (0.5–1 mm) are generally scarce (< 15% of the rock) but locally concentrated along decimetre-thick layers (Fig. 7c). Cordierite is restricted to the northern part of the study area (corresponding to the deepest structural levels) and the local occurrence of staurolite was reported in garnet–biotite schists near Ribes (Fig. 3,

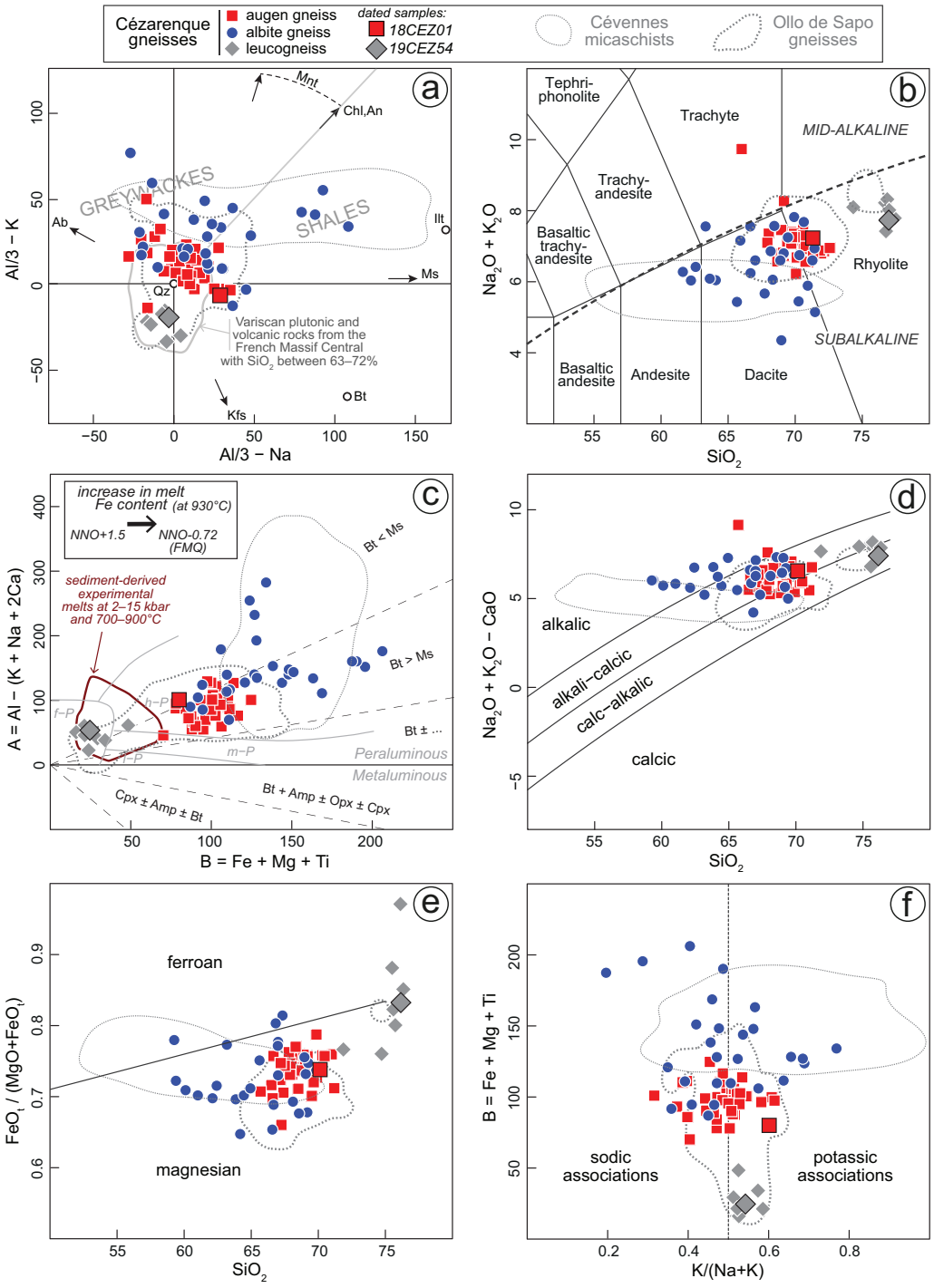

Fig. 6. Whole-rock geochemistry of the Cézarenque–Joyeuse gneisses. (a) Al/3-K *vs.* Al/3-Na cationic diagram of de La Roche (1968) aiming at discriminating meta-igneous from metasedimentary rocks. (b) Total alkali *vs.* silica classification diagram of Le Bas *et al.* (1986). The dashed line is the subalkaline–mid-alkaline boundary following Rittman (1957). (c) B–A cationic classification diagram of Debon and Le Fort (1988) with the subdivisions of Villaseca *et al.* (1998). (d) SiO_2 *vs.* $Na_2O + K_2O - CaO$ and (e) SiO_2 *vs.* $FeO_t/(FeO_t + MgO)$ (in wt.%) diagrams of Frost *et al.* (2001). (f) K/(K + Na) *vs.* B. cationic classification diagram of Debon and Le Fort (1988). The dotted lines represent the contours encompassing 85% of the data for the following distributions: Variscan plutonic and volcanic rocks from the French Massif Central with SiO_2 between 63–72% ($n = 1350$, Moyen *et al.*, 2017), the Ollo de Sapo gneisses ($n = 141$, based on the compilation of García-Arias *et al.*, 2018), the Cévennes mica schists ($n = 48$, data from Weisbrod, 1970; Harlaux, 2016; Couzinié, 2017). The contour levels were drawn using the kde2d function of R (Venables and Ripley, 2002). The B–A values for sediment-derived experimental melts at 2–15 kbar and 700–900 °C were taken from the compilation in Couzinié *et al.* (2017). The black arrow in (c) depicts the increase in Fe solubility observed by Gaillard *et al.* (2001) in a subaluminous 930 °C granitic melt when fO_2 decreases from NNO + 1.5 down to NNO-0.7 (~QFM, NNO sanding for Ni–NiO buffer).

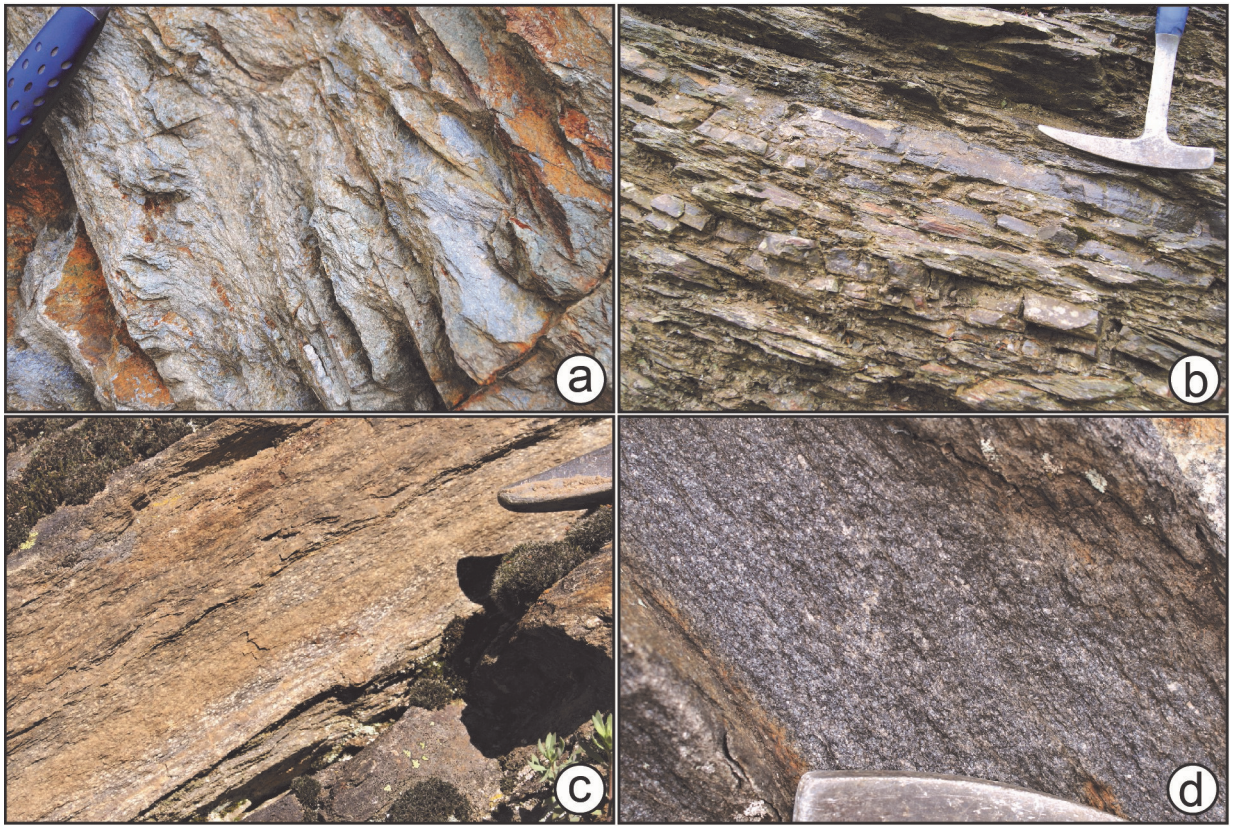

Fig. 7. Representative field photographs of the "Cévennes schists": (a) metapelitic chlorite–muscovite schist (44.5028°N, 4.1213°E); (b) schist with fine alternations of quartz-rich (poorly foliated) and quartz-poor domains (44.5833°N, 4.0545°E), likely derived from a semi-pelite protolith; (c) schist typified by layers rich in mm-sized albite porphyroblasts (44.5924°N, 3.9745°E); (d) dark (biotite-bearing) quartz schist, a facies primarily encountered close to the Cézarenque–Joyeuse gneisses (44.3937°N, 4.0781°E).

Bouilhol *et al.*, 2006). A peculiar dark-coloured quartz schist type, composed of fine-grained (sub-mm) quartz (> 80 vol.%), albite and biotite (Fig. 7d), was identified as 50 to 200 m-thick elongated bodies within the Cézarenque–Joyeuse gneisses.

3.3 Field relationships between the gneisses and the "Cévennes schists"

At the map scale, the contact between gneisses and the "Cévennes schists" is systematically parallel to the regional foliation and both lithologies appear interlayered. The gneisses define lenticular 10 to 250 m-thick bodies within the schists to the NE (near St-André and Ribes) and a larger massif to the S, reaching a thickness of ~2 km (Fig. 3). At the outcrop scale, contrasting relationships were observed. The contact is very often gradational, with albite gneisses progressively losing their feldspar load and grading to mica schists. In contrast, SE of Malons (Fig. 3), gneisses and schists are juxtaposed *via* a shear zone marked by the concentration of quartz lenses, intense folding, and the occurrence of mylonites. Asymmetric folds, interpreted as drag folds, consistently indicate a top-to-the NW transport, *i.e.*, thrusting of the gneisses over the schists (Fig. 4h), in agreement with the observations of Elmi *et al.* (1989) and Bouilhol *et al.* (2006). Finally, the eastern contact of the main gneiss massif is underlined by a distinctive decametric white quartzite (quartz > 95% vol.) layer (referred to as the "Peyremale" quartzite; Figs. 3 and 4g). The contact is sharp, parallel to the bedding in the quartzite (evidenced by grain-size variations) and can be followed along several kilometres.

Within the gneiss bodies, the transition between "augen" and "albite" types is very often gradational and intermediate facies do exist (Elmi *et al.*, 1989). Mapping of the augen gneiss-rich zones indicates that those are broadly concordant with the outline of the massif and the regional foliation. Conversely, the transposed contact between the leucogneisses and the augen gneisses, well-exposed in the Baume Valley (Fig. 3), is sharp and discordant (Fig. 4f), in agreement with the observations of Crevola *et al.* (1983), pointing to an intrusive relationship between the leucogneiss protolith and the augen gneiss protolith.

4 Zircon U–Pb dating and trace element compositions of the gneisses

Two representative Cézarenque–Joyeuse gneisses were selected for zircon U–Pb dating to clarify the age and origin of their protoliths. Both samples (augen gneiss 18CEZ01, and a tourmaline-bearing leucogneiss 19CEZ54, Figs. 4c and 4e) were collected from the Baume river cross-section (see Fig. 3).

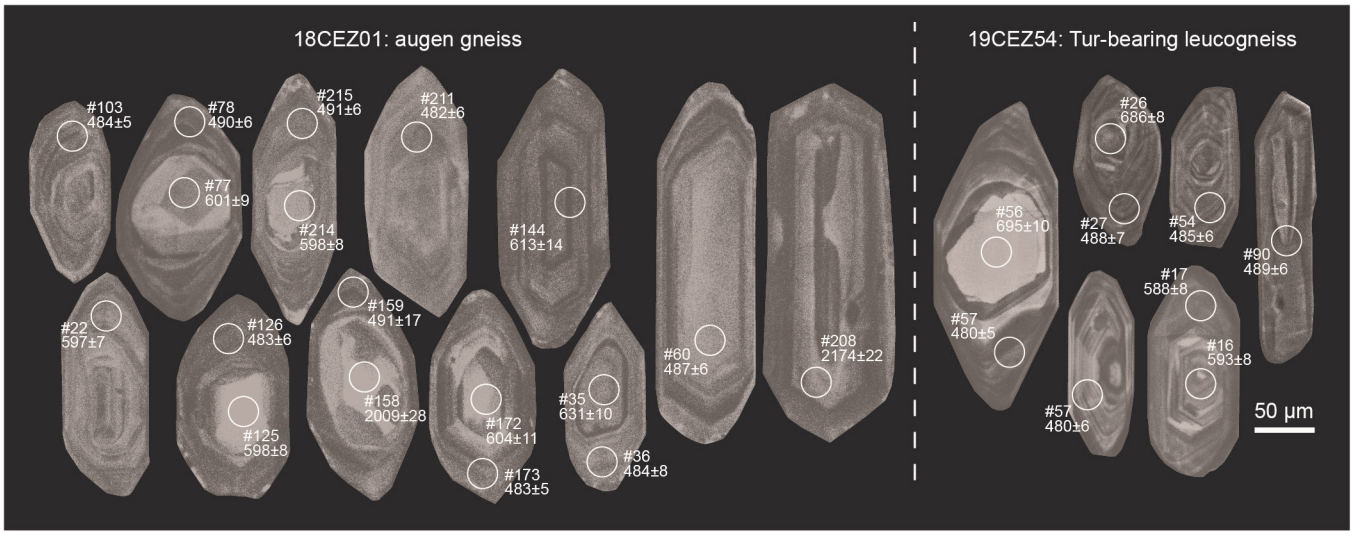

Fig. 8. Representative cathodoluminescence images of zircon grains from the Cézarenque gneisses. The locations of laser spots (white circles) are indicated along with the spot name (#XX). The corresponding $^{206}Pb/^{238}U$ dates (if < 1.2 Ga) or $^{207}Pb/^{206}Pb$ dates (if > 1.2 Ga) are quoted with 2σ uncertainty, in Ma. All displayed analyses are concordant.

4.1 Analytical techniques

Zircon grains were separated using standard techniques (jaw crusher, panning, heavy liquids), cast in epoxy resin and polished down to a near-equatorial grain section. Cathodoluminescence imaging was performed at the CRPG (Nancy, France) using a Jeol SM-6510 SEM equipped with a Gatan CL detector. Zircon U–Pb isotope and trace element analyses were carried out at ETH Zürich, Switzerland, by laser ablation–inductively coupled plasma–sector field–mass spectrometry using a RESOlution (ASI, Australia) 193 nm ArF excimer laser system attached to an Element XR (Thermo Scientific, Germany) mass spectrometer. Further details on the analytical procedures and the results of secondary standard and sample measurements are available in the Supplementary text and Supplementary Tables 2–5.

4.2 Zircon U–Pb dates

For the augen gneiss sample 18CEZ01, a total of 202 analyses were performed on 148 grains, most of which were euhedral, showed pyramidal tips and ranged in length between 150 and 300 µm with aspect ratios from 1:1.8 to 1:3.7. Cathodoluminescence imaging revealed that half of the grains were composed of a (often CL-bright) core wrapped around by a rim showing concentric oscillatory zoning (Fig. 8). Such rims yielded concordant $^{206}Pb/^{238}U$ dates comprised ($n = 38$) between 475 ± 7 (#164) and 498 ± 6 (#140) Ma. Three rims yielded older concordant dates of 525 ± 9 (#2), 575 ± 8 (#124), 621 ± 11 (#198) Ma. The discordant data ($n = 17$) showed a similar range of $^{206}Pb/^{238}U$ dates (Fig. 9). For 10 of them, elevated signals on mass 204 indicated that the discordance was at least partly related to common Pb incorporation. The core analyses ($n = 64$) yielded dominantly Neoproterozoic (40 concordant plus 4 discordant spots, $^{206}Pb/^{238}U$ dates from 542 ± 10 Ma, #55, up to 999 ± 13 Ma, #202) and Paleoproterozoic to Neoarchean dates (14 concordant and 7 discordant spots, with $^{207}Pb/^{206}Pb$ between 1870 ± 47, #50, and 2718 ± 25 Ma, #218). One core yielded a concordant Paleoarchean date of 3282 ± 17 Ma (#20), making it the oldest concordant analysis so far obtained in the eastern Massif Central (see Chelle-Michou *et al.*, 2017; Couzinié *et al.*, 2019). The remaining 73 grains lacked any core–rim relationship and showed well-developed concentric magmatic oscillatory zoning. Thirty-seven analyses yielded concordant to slightly discordant $^{206}Pb/^{238}U$ dates clustered between 479 ± 5 Ma (#213) and 499 ± 7 Ma (#170). In contrast, 34 grains yielded concordant to slightly discordant Lower Cambrian to Neoproterozoic dates between 526 ± 8 Ma (#167) and 753 ± 15 Ma (#92) and 4 grains (2 discordant) showed $^{207}Pb/^{206}Pb$ dates of 1898 ± 30 (#106) to 2174 ± 22 Ma (#179). Seven analyses were strongly discordant and not considered further.

For the tourmaline-bearing leucogneiss sample 19CEZ54, 100 analyses were performed on 68 grains which appeared often broken, slightly corroded and of smaller size (130–170 µm, rarely up to 250 µm) than in sample 18CEZ01. Aspect ratios of euhedral unbroken grains were also more variable and generally comprised between 1:2.2 and 1:2.8 but up to 1:5 in some cases. Fifty-two analyses were performed on grains devoid of core-rim relationships but showing prominent concentric oscillatory zoning (striped zoning in the most elongated grains). The concordant analyses clustered between 468 ± 6 (#68) and 489 ± 6 (#90) Ma ($n = 24$) with 2 grains showing younger dates of 428 ± 12 (#75) and 433 ± 9 (#94) Ma and 12 grains older dates from 545 ± 6 (#44) to 611 ± 9 (#86), up to 1212 ± 6 (#76) Ma. Out of the 16 discordant $^{206}Pb/^{238}U$ dates obtained, 8 overlapped with the concordant data (490–480 and at c. 540 Ma) while 8 defined a continuous trend from 455 ± 7 (#87) to 414 ± 6 (#36) Ma. The remaining analyses were performed on grains comprising a relict core surrounded by oscillatory-zoned overgrowths. Eleven rims yielded concordant overlapping $^{206}Pb/^{238}U$ dates between

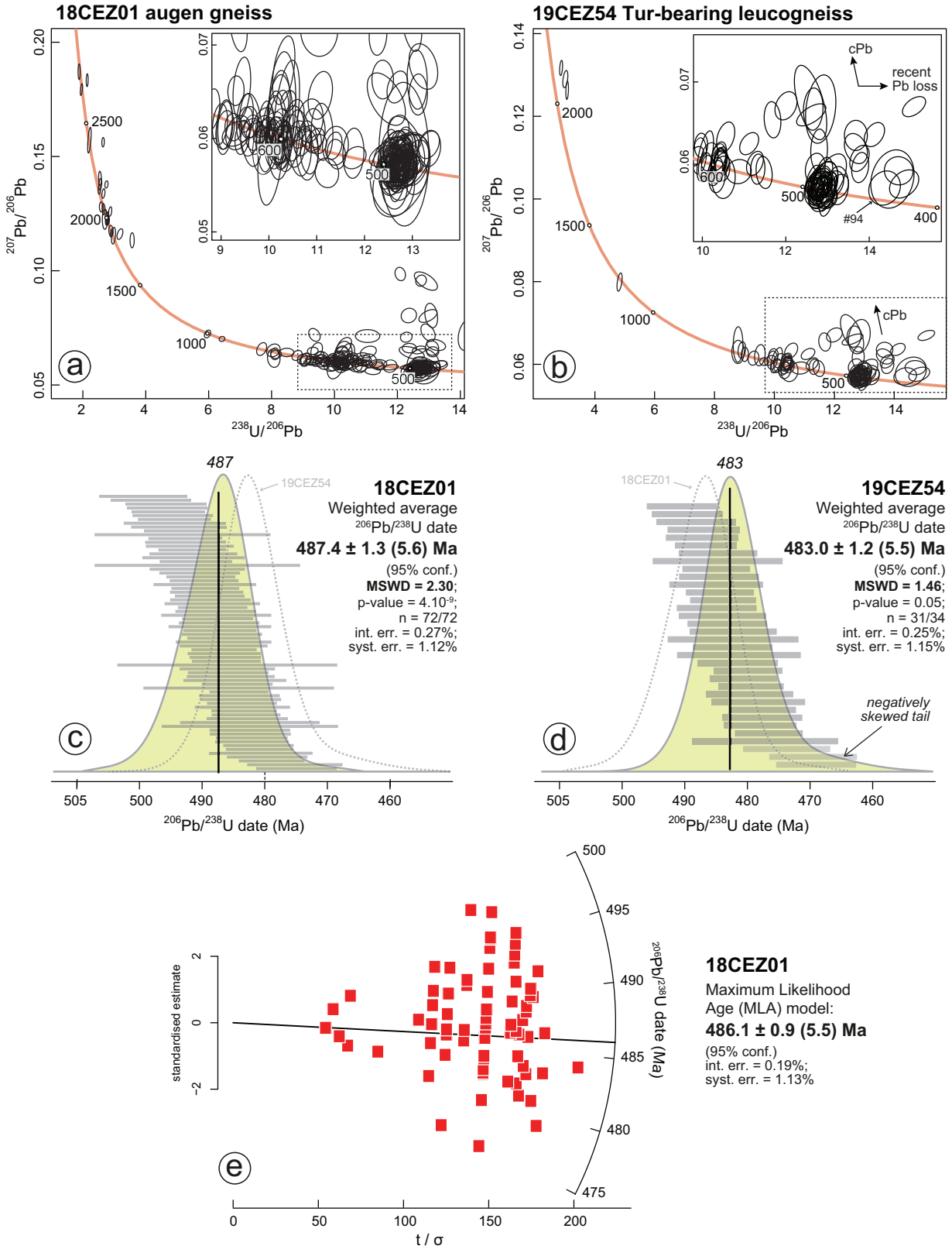

Fig. 9. Zircon U–Pb results for the Cézarenque gneiss samples. (a,b) Tera–Wasserburg diagrams ($^{238}U/^{206}Pb$ *vs.* $^{207}Pb/^{206}Pb$). Error ellipses/ages are quoted at the 95% confidence level. Analyses were not corrected from common Pb. (c,d) Individual Furongian–Lower Ordovician $^{206}Pb/^{238}U$ dates (grey bars) and their distributions represented as Kernel Density Estimates (with an adaptative bandwidth). Only concordant data were considered. (e) Radial plot and Maximum Likelihood Age estimate for sample 18CEZ01 (see Vermeesch, 2021).

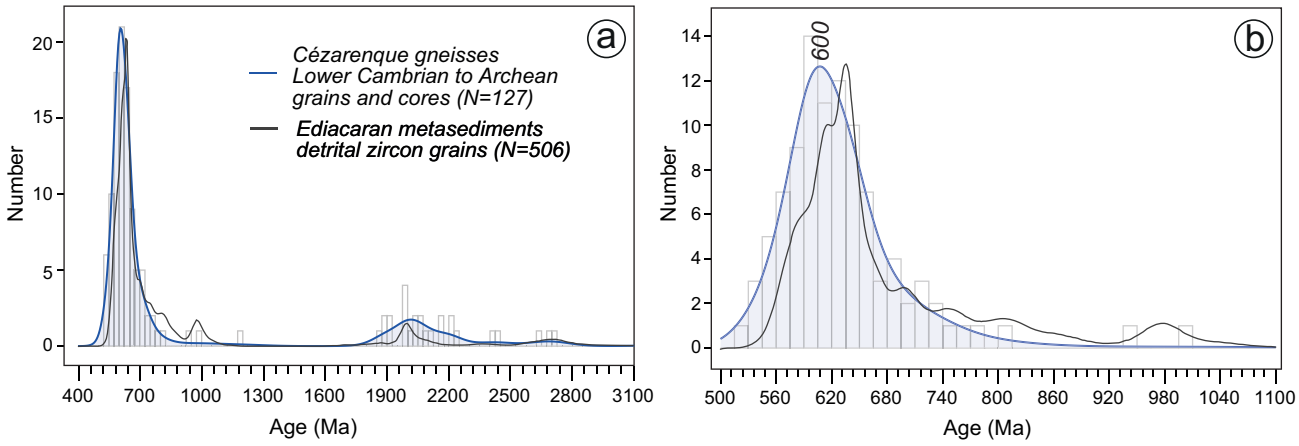

Fig. 10. Histograms and Kernel Density Estimates (plotted with an adaptive bandwidth) showing the U–Pb date distribution of older-than-Lower Cambrian zircon grains, rims, and cores from the Cézarenque–Joyeuse gneisses. Only concordant $^{206}Pb/^{238}U$ dates (if < 1.2 Ga) and concordant to slightly discordant ("$^{206}Pb/^{238}U$ date"/"$^{207}Pb/^{206}Pb$ date" > 92%, if > 1.2 Ga) were considered. The data are compared to the U–Pb date distribution of Ediacaran metasediments from the Cévennes parautochthon of the eastern Massif Central, also represented as Kernel Density Estimates (Chelle-Michou *et al.*, 2017: Couzinié *et al.*, 2019).

480 ± 5 (#57) and 490 ± 6 (#41) Ma and a discordant date of 356 ± 6 (#96) Ma. The 24 analysed cores showed concordant to slightly discordant $^{206}Pb/^{238}U$ dates between 492 ± 11 (#52, disc.) and 695 ± 10 (#82) Ma (16 concordant, 3 discordant) with 3 cores having older slightly discordant $^{207}Pb/^{206}Pb$ dates of 2045 ± 25 (#95) to 2119 ± 20 (#37) Ma. Out of the 27 discordant analyses, 16 showed detectable signals on mass 204 suggesting that discordance was at least partly related to common Pb incorporation.

To sum up, both gneiss samples were typified by the occurrence of oscillatory-zoned grains and rims with $^{206}Pb/^{238}U$ dates in the range 475–500 Ma, *i.e.*, Furongian–Tremadocian (Fig. 9). The cores and the remaining oscillatory-zoned grains generally displayed Lower Cambrian–Neoproterozoic (525–999 Ma, peak at 600 Ma, Fig. 10b) and Paleoproterozoic–Neoarchean dates (1.8–2.7 Ga). For sample 18CEZ01, the density distribution of the Furongian–Tremadocian dates ($n = 72$) was clearly symmetrical, centred on 487.4 Ma but importantly, the results of a χ^2_{red} test for homogeneity indicated that the data were overdispersed given the estimated analytical uncertainties (MSWD = 2.3, p-value of 10^{-9}) (Fig. 9). This overdispersion is due to the 5 youngest and 5 oldest dates of the population. Alternatively, the statistical procedure of Montel *et al.* (1996) shows that the data can be modelled as a mixture of two populations, one centred at 492.2 ± 1.3 Ma ($n = 46$) and the other at 484.2 ± 1.0 Ma ($n = 27$, with global p-value of 0.94). The grains belonging to each population are undistinguishable based on texture or trace element compositions. For sample 19CEZ54, 34 analyses clustered in the range 490–468 Ma. Their distribution was asymmetrical and negatively skewed (towards younger ages). Excluding the three youngest analyses allowed to calculate a weighted average date of 483.0 ± 1.2 Ma (± 5.5 after propagation of systematic uncertainties) with an MSWD of 1.46 (p-value = 0.05) indicating that the considered grains may sample a single population.

4.3 Zircon trace element compositions

Only compositions obtained from concordant U–Pb spots will be presented and further discussed, summing up to 159 spots for the augen gneiss 18CEZ01 and 64 for the leucogneiss 19CEZ54. Eu/Eu* were calculated as $Eu_N/(Sm_N \times Gd_N)^{0.5}$ but Ce/Ce* as $(Nd_N)^2/Sm_N$ following the approach of Loader *et al.* (2017). Since this method does not rely on the La and Pr contents, it is less sensitive to presence of minute inclusions of apatite, monazite or xenotime which would flaw the LREE budget of the analysed zircon grain and lead to inaccurate estimates of Ce/Ce* (*e.g.*, Ni *et al.*, 2020). In the formulas, the $_N$ stands for "normalized to the chondritic values", here of Boynton (1984). Ranges given in the description below correspond to the 1st and 3rd quartiles of the distribution unless stated otherwise.

For the augen gneiss 18CEZ01, all grains no matter their age or texture showed relatively steep HREE patterns with $(Dy/Yb)_N$ mostly between 0.15–0.25 (Figs. 11a and 11c), and a variable range of Ti contents (4.4–9.5 ppm). Furongian–Tremadocian grains and rims displayed very consistent trace element signatures that strongly contrasted with that of the Lower Cambrian/Neoproterozoic and Paleoproterozoic/Neoarchean grains and cores (Fig. 11). They were typified by lower Th/U ratios (0.03–0.13 *vs.* 0.30–0.74 and 0.53–0.92, respectively), lower LREE contents (Ce: 0.3–1.3 *vs.* 5.6–19.1 and 10.8–21.4 ppm; Nd: 0.4–1.1 *vs.* 0.8–2.4 and 1.3–5.2 ppm), deeper Eu negative anomalies (Eu/Eu*: 0.04–0.08 *vs.* 0.13–0.37 and 0.06–0.15) and less pronounced Ce positive anomalies (Ce/Ce*: 5–10 *vs.* 21–100 and 11–37).

A similar situation was observed in leucogneiss sample 19CEZ54 (Fig. 11) with all grains exhibiting steep HREE patterns (with $(Dy/Yb)_N$ centred around 0.16–0.25) and variable Ti contents (5.4–10.3 ppm). The Furongian–Tremadocian grains and rims had nearly identical trace element

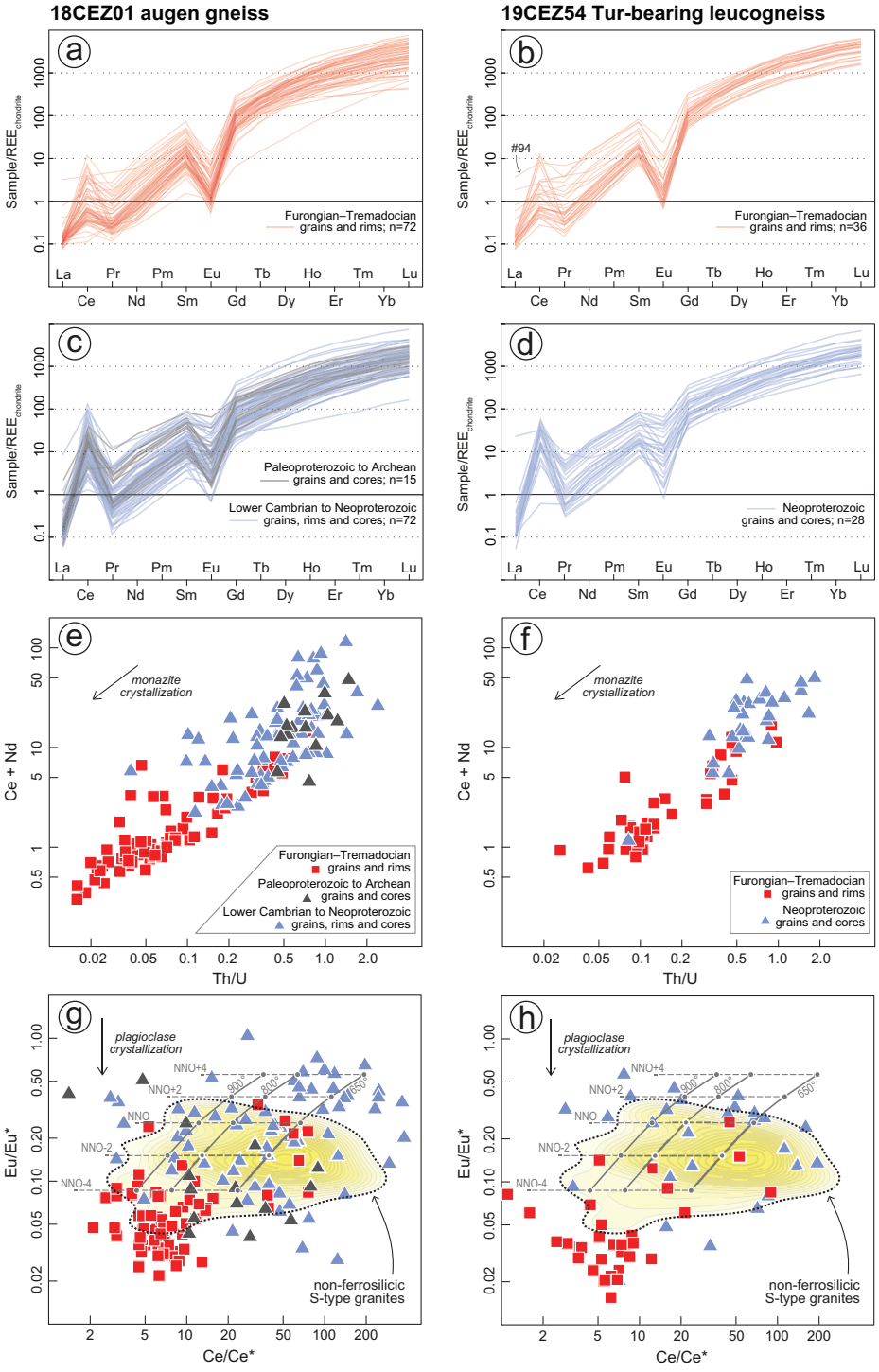

Fig. 11. Zircon trace element data for the Cézarenque–Joyeuse gneisses. (a,b,c,d) Rare Earth Elements patterns normalized to the chondrite values of Boynton (1984); (e,f) LREE contents (Ce + Nd) *vs.* Th/U diagram for the different date populations; (g,h) Eu/Eu* *vs.* Ce/Ce* diagram. The background yellow shading mimics the contours of the distribution of 209 zircon analyses from S-type granites which whole-rock compositions are not ferrosilicic (data from Wang *et al.*, 2012: Gao *et al.*, 2016: Burnham and Berry, 2017), drawn using the kde2d function of R (Venables and Ripley, 2002). For sake of consistency, Ce/Ce* of the literature zircon were recalculated using the same methodology as for the Cézarenque–Joyeuse gneisses, *i.e.*, following the approach of Loader *et al.* (2017). Were also plotted the relationships between zircon Eu and Ce anomalies and melt temperature–oxygen fugacity, as estimated by Trail *et al.* (2012) for peraluminous melt compositions. The oxygen fugacity (fO_2) in this plot is expressed relative to the NNO (nickel–nickel oxide) buffer. At 800 °C, the fO_2 of the quartz–fayalite–magnetite (QFM) buffer corresponds to NNO-0.8 and that of the iron–wüstite buffer is NNO-5.

compositions than those extracted from 18CEZ01 which, here again, markedly contrasted with the signature of Neoproterozoic grains and cores. Their Th/U and LREE contents were systematically lower (Th/U: 0.08–0.32 *vs.* 0.49–0.85; Ce: 0.5–2.1 *vs.* 10.2–27.1 ppm; Nd: 0.6–1.7 *vs.* 1.3–5.5 ppm), the Eu negative anomalies were more pronounced (Eu/Eu*: 0.03–0.06 *vs.* 0.13–0.33) and the Ce positive anomalies weaker (Ce/Ce*: 5–9 *vs.* 16–71). Collectively, this indicates that the Furongian–Tremadocian and the older-than-Lower-Cambrian zircon grains crystallized in magmas of contrasted chemical compositions.

4.4 Ti-in-zircon and zircon saturation thermometry

The crystallization temperatures of Furongian–Tremadocian zircon grains and rims were calculated from their Ti contents using the equation of Ferry and Watson (2007) with a_{SiO2} of 1 and a_{TiO2} of 0.5 as suggested by Schiller and Finger (2019) for S-type felsic magmas. In both samples, estimated values spread over a large range of temperatures (between 670 and 900 °C) but with a main cluster at 730–770 °C (Fig. 12).

Zircon saturation temperatures were obtained based on the major element and Zr contents of the dated samples using the equation of Watson and Harrison (1983). A melt having a composition akin to augen gneiss sample 18CEZ01 would be saturated in zircon below 844 ± 42 °C (considering a 5% absolute uncertainty). A lower temperature of 721 ± 36 °C was retrieved for the leucogneiss sample. Given the common preservation of zircon cores in both samples, these values should be regarded as maximum magma temperatures.

5 Discussion

5.1 Nature and age of the protoliths of the Cézarenque–Joyeuse gneisses

5.1.1 Interpretation of the field relationships, petrography, and whole-rock compositions

Three models exist regarding the origin of the Cézarenque–Joyeuse gneisses: (a) they represent metasediments (conglomerates and arkoses) reworking materials of igneous origin (granite pebbles, microcline clasts, Weisbrod and Marignac, 1968); (b) they are metagranites (Crevola *et al.*, 1983); (c) they correspond to volcanic and volcano-sedimentary rocks (Chenevoy, 1968a, 1968b; Faure *et al.*, 2001). Model (a) should be discounted as a significant proportion of the gneisses (the augen facies and at least a third of the albite gneisses) show acidic *igneous* compositions (see Sect. 3.1). Model (c) is preferred against model (b) as the latter cannot explain the gradual transition at the outcrop scale from rocks of igneous *vs.* sedimentary (two thirds of the albite gneisses) origin. The volcanic model is also supported by the elevated normative Qz/(Ab + Or) ratios (average of 0.66) of the igneous samples consistent with a low pressure of crystallization of their parental magmas (Wilke *et al.*, 2017) and the sharp, stratigraphic, contact between the gneisses and the overlying Peyremale quartzite (see Sect. 3.3), pointing to a near-surface emplacement.

In this frame, based on the SiO_2–alkalis systematics (Fig. 5b), we infer that the augen and albite gneisses with igneous compositions represent now-metamorphosed rhyodacites. Their blue quartz grains and pseudomorphs after K-feldspar (for the augen facies) embedded in a finer grained matrix are regarded as former igneous phenocrysts, a view consistent with the fact that the blue colour of quartz is commonly interpreted as resulting from rutile exsolution from grains crystallized at high temperature (T > 700 °C, Seifert *et al.*, 2011). The persistence of blue quartz grains in the albite gneisses of sedimentary origin and their composition akin to greywackes indicate that they represent the proximal remobilization products of the adjacent rhyodacites, *i.e.*, epiclastic tuffs. Finally, the leucogneisses are strongly silicic and show a large range of Fe/Mg ratios (Fig. 6) which are typical of fractionated granitic melts. Given their cross-cutting field relationships and their elevated normative Qz/(Ab + Or) ratios (again pointing to crystallization at low pressure), they likely represent former microgranite dykes intrusive within the rhyodacites and associated epiclastic tuffs.

5.1.2 Interpretation of U–Pb results

In line with the abovementioned arguments, the augen gneiss sample 18CEZ01 should be regarded as a metamorphosed porphyritic (K-feldspar-bearing) rhyodacite and the leucogneiss sample 19CEZ54 as a metamicrogranite. In the following, only concordant zircon analyses will be discussed, discordant results being ascribed to a combination of common Pb incorporation and Pb loss.

The augen gneiss (metarhyodacite) 18CEZ01 contains many magmatic grains and rims yielding Furongian–Tremadocian $^{206}Pb/^{238}U$ dates, the distribution of which is well-centred around 487 Ma and would correspond to the crystallization age of the magma. Importantly, considering the estimated analytical uncertainties, the dates are statistically overdispersed. The lack of correlation between U contents and $^{206}Pb/^{238}U$ dates and the symmetrical shape of the date distribution collectively suggest that this overdispersion is of geologic significance (Spencer *et al.*, 2016) and should not be ascribed to limited Pb loss. In line with the volcanic origin of 18CEZ01, it is likely that the analysed dataset comprises syn-eruptive zircon grains and rims plus antecrysts which formed in deep-seated magma chambers (*e.g.*, Matzel *et al.*, 2006) and were scavenged during the eruption. For such cases (mixture of pre-eruptive and syn-eruptive grains, undistinguishable on textural and chemical grounds), Vermeesch (2021) argued that the "Maximum Likelihood Age" (MLA) model designed by Galbraith (2005) has a high potential to unravel the actual crystallization age of the igneous rock. Indeed, the MLA model presumes that the antecrysts define a continuous range of pre-eruptive dates, which is arguably more realistic than the "two populations" (*i.e.*, two age clusters) subdivision (see Sect. 4.2) inferred based on the statistical procedure of Montel *et al.* (1996). Running the MLA algorithm yields 486.1 ± 0.9 Ma (± 5.5 Ma when systematic uncertainties are considered), which is the best estimate of the eruption age of the augen gneiss parental magma. We interpret the grains and cores showing older dates (from the Lower Cambrian to Paleoarchean) as inherited from the magma source or as xenocrysts incorporated from the country-rocks during magma ascent and emplacement (Fig. 9).

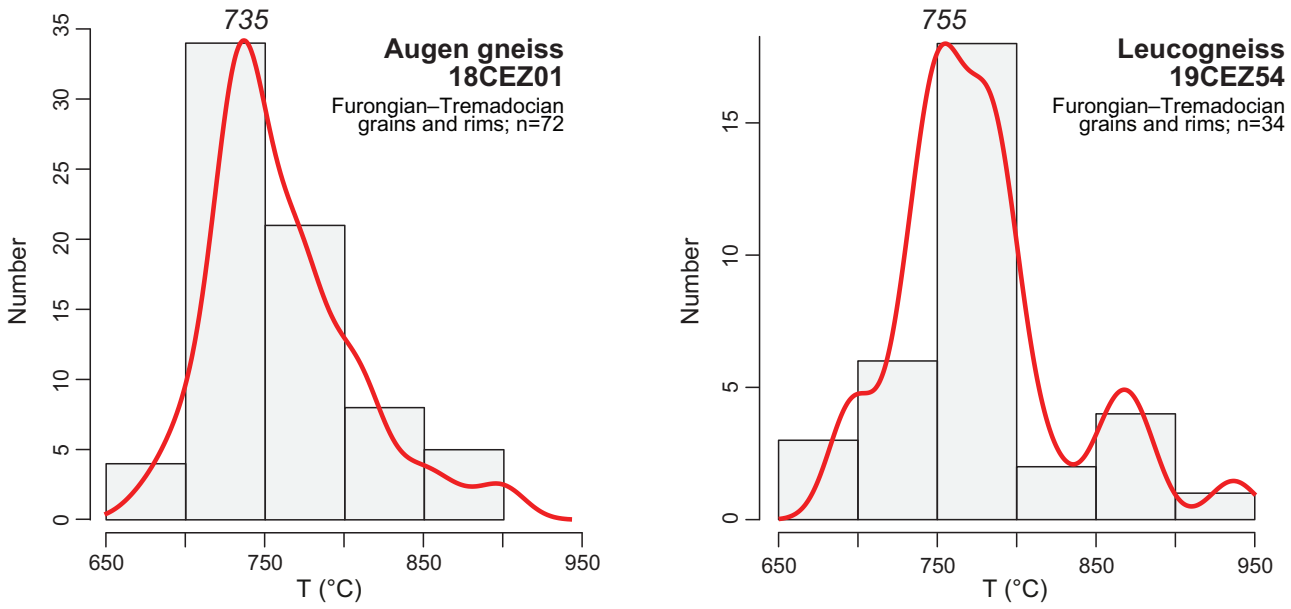

Fig. 12. Histograms and density distribution of temperatures for magmatic Furongian–Lower Ordovician grains and rims of the Cézarenque–Joyeuse gneisses, obtained *via* the Ti-in zircon thermometer using the equation of Ferry and Watson (2007) with a_{SiO2} of 1 and a_{TiO2} of 0.5 as suggested by Schiller and Finger (2019) for peraluminous felsic magmas.

For the metamicrogranite 19CEZ54, most oscillatory-zoned grains and rims also yielded $^{206}Pb/^{238}U$ dates in the range 475–500 Ma with two concordant analyses showing overlapping younger dates of 428 ± 12 Ma (#75) and 433 ± 9 Ma (#94). We do not ascribe any significance to these dates because in both cases the $^{206}Pb/^{238}U$ date / $^{207}Pb/^{206}Pb$ date ratios are < 90%, hence suggesting post-magmatic disturbance of the isotopic system (Spencer *et al.*, 2016). Besides, the grain domain corresponding to analysis #94 showed elevated Ti (~160 ppm), Nb–Ta (9 and 10 ppm, respectively) and Pr contents (0.8 ppm), which are an order of magnitude higher than in other zircon grains and likely attests to the presence of zirconolite, a common product of zircon alteration (Gieré, 1996). Excluding these two dates, we infer that the cluster at c. 483 Ma represents the crystallization age of the parental magma, in agreement with textural evidence. Importantly, the negatively skewed distribution argues for the occurrence of Pb loss from the 475–500 Ma magmatic population (Spencer *et al.*, 2016) and, excluding the 3 youngest dates, we retain the weighted average date of 483.0 ± 1.2 Ma (± 5.5 Ma considering systematic uncertainties) as the best estimate of the crystallization age of the microgranite protolith.

The difference of 3 Ma between zircon crystallization ages in the two felsic magmas exceeds the internal uncertainties and, since both samples were dated during the same analytical session, such time interval may be of geological significance (Horstwood *et al.*, 2016). The slightly younger crystallization age of the microgranite 19CEZ54 is consistent with field observations supporting an intrusive relationship with the porphyritic metarhyodacite 18CEZ01.

5.2 Typology and petrogenesis of the igneous association

Nearly overlapping crystallization ages and key geochemical markers (including almost identical whole-rock Na/K ratios, Fig. 6d, and similar magmatic zircon trace element systematics, Fig. 11) collectively indicate that the metarhyodacites and the metamicrogranites were genetically related and constitute a single magmatic system. Considered together, they define a peraluminous, calc-alkalic to alkali-calcic, magnesian and sodi-potassic association (Fig. 6), which is the hallmark of crust-derived magmatic suites (Bonin *et al.*, 2020). Further evidence for a crustal origin is provided by the marked zircon inheritance (Laurent *et al.*, 2017) and zircon trace element systematics. Indeed, the low Th/U ratios displayed by the magmatic zircon grains, positively correlated with LREE contents (Figs. 11e and 11f), can be regarded as a consequence of coeval monazite precipitation from the melt upon cooling which is a typical feature of highly aluminous and P-rich "S-type" granitic melts formed by melting of sedimentary rocks (Cuney and Friedrich, 1987). Besides, as Ce^{4+} and Eu^{3+} are less incompatible with respect to zircon than Ce^{3+} and Eu^{2+} (*e.g.*, Trail *et al.*, 2012, and references therein), the low Ce/Ce* and Eu/Eu* ratios (weak Ce positive anomalies and marked Eu negative anomalies, Figs. 11g and 11h) displayed by magmatic zircon grains demonstrate that the parental magmas were notably reduced, as commonly observed in S-type granitic melts (Whalen and Chappell, 1988).

Examination of the inherited zircon date distributions and trace element systematics sheds light on the nature and origin of the crustal source. The main Neoproterozoic

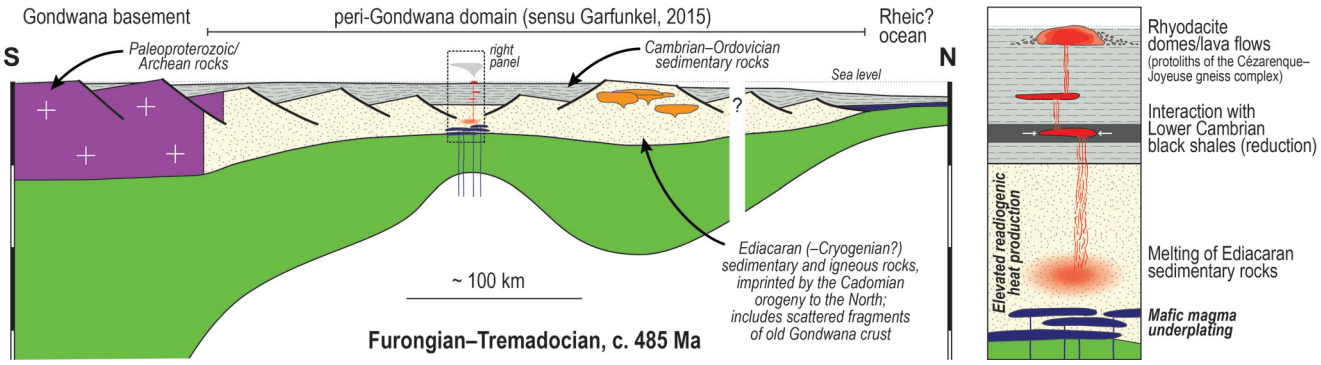

Fig. 13. Interpretative geodynamic sketch illustrating the Furongian–Lower Ordovician evolution of the northern Gondwana margin. The crustal column on the right panel summarises the petrogenetic model proposed for the protoliths of the Cézarenque–Joyeuse gneiss complex.

(Ediacaran–Cryogenian, 541–720 Ma) and subordinate Paleoproterozoic (1.9–2.2 Ga) clusters are remarkably matching those observed in Ediacaran metasediments from deeper structural levels of the Cévennes domain (Chelle-Michou *et al.*, 2017; Couzinié *et al.*, 2019) which strongly suggests that the Cézarenque–Joyeuse magmas formed by melting of Ediacaran sedimentary rocks. The occurrence of two inherited grains showing overlapping c. 525 Ma U–Pb dates indicates that the magmas interacted at some point of their evolution with a Lower Cambrian crustal component, possibly during ascent (in which case these zircon grains are xenocrysts).

Interestingly, the inherited Precambrian grains have a wider range of trace element compositions compared to magmatic grains and include a significant proportion of zircon with higher Th/U and LREE contents together with stronger positive Ce anomalies and weaker Eu negative anomalies. These latter signatures suggest that the Precambrian igneous rocks which erosion products fed the Ediacaran sedimentary basins largely originated from more oxidised (Figs. 11g and 11h), probably arc-derived magmas (Ishihara, 2004). For the Neoproterozoic grains, the long-lived accretionary Cadomian orogeny, developed along the northern Gondwana margin (Garfunkel, 2015, and references therein), constitutes the most likely source. The Paleoproterozoic to Archean zircon grains would stem from the recycling of old Gondwanan crustal materials, possibly originating from the Saharan Metacraton (Couzinié *et al.*, 2019).

The Cézarenque–Joyeuse felsic igneous rocks have whole-rock compositions matching those of the so-called *ferrosilicic* suites (Castro *et al.*, 2009), *i.e.*, they are anomalously rich in Fe and Mg and low in Ca. Such signatures have been thought to result from very high melting temperatures (> 1000 °C) of sedimentary rocks (mostly greywackes, Castro *et al.*, 2009). However, several observations argue against this model for the Cézarenque–Joyeuse gneisses. First, a large pool of inherited zircon grains and cores were preserved throughout the magmatic evolution implying either moderate melting temperatures (< 850 °C, below the zircon saturation temperature of the augen gneiss) or very fast melt production and transfer to the upper crust (Watson, 1996; Bea *et al.*, 2007). In the latter case, the magmas are expected to have followed a nearly adiabatic path from source to surface. This way, crystallization temperatures deduced from Ti-in-zircon thermometry (clustering at 730–770 °C, see Sect. 4.4) should lie within 50 °C of the actual melting temperatures (Holtz and Johannes, 1994), which, therefore, could not have exceeded 820 °C. As an alternative to the very high melting temperature model, Fiannacca *et al.* (2019) suggested that the *ferrosilicic* signature should be explained by the selective incorporation in the melt phase of mafic materials (mostly peritectic garnet, Stevens *et al.*, 2007) present in the sedimentary source. Yet appealing, this model cannot be directly tested in that any petrographic evidence for such entrainment was irremediably erased during the dissolution of the added crystal load.

Novel insights on the origin of the *ferrosilicic* signature may be gained from the examination of the Eu/Eu* and Ce/Ce* systematics of the Cézarenque–Joyeuse magmatic zircon grains and rims. Measured values (Figs. 10g and 10h) are significantly lower compared to zircon encountered in "typical" (not *ferrosilicic*) sediment-derived granites from the Lachlan Fold Belt (Burnham and Berry, 2017) and southern Tibet (Wang *et al.*, 2012; Gao *et al.*, 2016), calling for anomalously reducing conditions. The fO_2 prevailing during zircon crystallization was most likely close to the value expected for the iron–wüstite buffer considering the calibration of Trail *et al.* (2012). Little is known on the influence of fO_2 on anatectic melt compositions, but Gaillard *et al.* (2001) showed that the Fe solubility of a subaluminous (A/CNK between 1 and 1.1) melt at 930 °C is negatively correlated to fO_2: at NNO + 1.5, maximal FeO_t contents reach ~1.8 wt.% but are higher than 3 wt.% at fO_2 below FMQ. Since the alumina content of a granite melt at a given fO_2 has no influence on the Fe solubility (Holtz *et al.*, 1992), this result should also be valid for peraluminous melt compositions. Hence, we posit that the high Fe contents displayed by the *ferrosilicic* rocks may result from an enhanced Fe solubility in the melt phase itself caused by strongly reducing conditions. Those may be inherited from the source level (melting in a graphite-buffered environment) or acquired during ascent *via* interaction with organic matter (possibly oil-bearing) sedimentary rocks, a phenomenon known to deeply affect the fO_2 of magmas (*e.g.*, Iacono-Marziano *et al.*, 2012). As a matter of fact, the Lower Cambrian sequences of the southern Massif Central *autochthon* host a > 200 m-thick black shale formation (Álvaro *et al.*, 2014), to which graphite-bearing mica schists of the Cévennes parautochthon may be correlated. Hence, the low fO_2 and

peculiar high Fe contents of the Cézarenque–Joyeuse parental magmas may result from their interaction with the local Lower Cambrian sediments prior to the eruption (Fig. 13).

5.3 The Cézarenque–Joyeuse magmatism in the frame of the northern Gondwana evolution

Felsic (sub)volcanic and volcanosedimentary associations coeval to the Cézarenque–Joyeuse gneisses are widespread over the northern Gondwana terrains of SW Europe. In this section, we first provide a short review of correlative formations and then address the geodynamic setting and the trigger(s) of this magmatic flare-up.

The best-characterized Furongian–Lower Ordovician metavolcanic suite of the northern Gondwana realm is arguably the Ollo de Sapo Formation in the Iberian Massif (see review in García-Arias *et al.*, 2018; von Raumer and Stampfli, 2018). The Ollo de Sapo gneisses strikingly resemble their Cezarenque–Joyeuse counterparts: lithological types (augen *vs.* fine-grained facies) and whole-rock chemical compositions are alike (Fig. 6), as already noted by Weisbrod (1969); their ages overlap within uncertainty (Montero *et al.*, 2007, 2009, 2017; Díez Montes *et al.*, 2010; Lopez-Sanchez *et al.*, 2015); the same petrogenetic model is inferred, *i.e.*, melting of Ediacaran sedimentary rocks (Montero *et al.*, 2017). Additional correlations can be established with several massifs exposed throughout the Variscan nappe pile: (i) in the Massif Central (Fig. 1), the Cézarenque–Joyeuse gneisses recall the metarhyolites from the St-Salvi-de-Carcavès–St-Sernin-sur-Rance and Thiviers–Payzac units (Guérangé-Lozes and Burg, 1990; Melleton *et al.*, 2010; Álvaro *et al.*, 2014; Pouclet *et al.*, 2017) and from the Indre group (Nouzier metavolcanics, Quesnel *et al.*, 2009); (ii) in the Armorican Massif, they resemble the felsic rocks from the "Porphyroid nappe" and the Brétignolles, Île de Groix and La Châtaigneraie metavolcanics (Bouton and Branger, 2008; Ballèvre *et al.*, 2012; El Korh *et al.*, 2012); (iii) in the Iberian Massif, besides the Ollo de Sapo Formation, they are akin to several metarhyolites bodies exposed in the parautochthonous "Schistose Domain" (Valverde-Vaquero *et al.*, 2005; Dias Da Silva *et al.*, 2014; Farias *et al.*, 2014); (iv) in Sardinia, they compare to the volcanics of the San Vito Formation and the Li Trumbetti and Mt. Geisgia rhyolites (Oggiano *et al.*, 2010). Furthermore, many peraluminous crust-derived (meta)granites of similar Furongian–Lower Ordovician age have been described in the same areas and possibly represent former deep-seated magma reservoirs that fed the eruptions (Álvaro *et al.*, 2020a, b). Relevant examples include the Mendic pluton in the Massif Central (Demange, 1982; Álvaro *et al.*, 2014; Pouclet *et al.*, 2017), the Mervent orthogneiss in the Armorican massif (Diot *et al.*, 2007) and numerous massifs in Iberia (Díez Fernández *et al.*, 2012; Talavera *et al.*, 2013).

Altogether, petrological and geochronological evidence substantiate that a pervasive crustal melting event took place along a >2000 km segment of the northern Gondwana margin (Álvaro *et al.*, 2020a, b). From a geodynamic perspective, an intracontinental rift setting (Fig. 13) should be retained based on: (i) the linear shape of the magmatic belt and the synchronous deposition of thick sedimentary sequences (Pouclet *et al.*, 2017); (ii) the occurrence of "anorogenic" A-type magmatic rocks in NW Iberia (Díez Fernández *et al.*, 2012, and references therein), in the Maures massif (Seyler, 1986; Briand *et al.*, 2002), in the Armorican Massif (Ballèvre *et al.*, 2012) and in the southern Massif Central (Albigeois area, Pin and Marini, 1993); (iii) the lack of regional metamorphism related to crust thickening (*e.g.*, Montero *et al.*, 2007); and (iv) the coeval opening of the Rheic ocean (Díez Montes *et al.*, 2010; Nance *et al.*, 2010). The ultimate origin of this rifting event remains debated. Many authors put forward the role of the southwards (in Ordovician coordinates) subducting Iapetus slab in controlling crustal extension (Fernández *et al.*, 2008; Díez Montes *et al.*, 2010; Díaz-Alvarado *et al.*, 2016; Oriolo *et al.*, 2021) while others retained a plume-induced origin (Briand *et al.*, 1992, 2002). The geological record of the Cévennes parautochthon does not provide any evidence that would help clarify this point.

An atypical feature of this rifting event is the voluminous generation of peraluminous crust-derived magmas, which are more commonly encountered in syn- to post-collisional orogenic settings (Barbarin, 1999). Two factors seem to have played a key role in enabling the crust to produce granitic melts under such conditions. First, evidence for mantle-derived magma underplating and associated advective/conductive heat transfer are provided by the occurrence of coeval mafic magmatic rocks in the vicinity of the felsic volcanic centres (Bea *et al.*, 2007; Montero *et al.*, 2009; Díez Montes *et al.*, 2010; Díaz-Alvarado *et al.*, 2016; Pouclet *et al.*, 2017). However, such rocks represent small volumes compared to the felsic suites and are not systematically exposed (*e.g.*, in the Cézarenque–Joyeuse area) thus calling for an additional heat supply. As a matter of fact, the thick Ediacaran sedimentary sequences which constitute the source rocks of the Furongian–Lower Ordovician magmas were characterized by anomalously high radiogenic heat productions: $>2.7\ \mu W.m^{-3}$ at 550 Ma in the Iberian "Schist and Greywacke Complex" (Bea *et al.*, 2003) and average of $3.0\ \mu W.m^{-3}$ in the Massif Central (Couzinié, 2017), *i.e.*, 50% higher than the mean upper crustal composition of Rudnick and Gao (2003). This feature was explained by the recycling of Cadomian felsic igneous rocks which selectively enriched the Ediacaran detritus in K, Th and U (Bea *et al.*, 2003). Numerical modelling indicates that the presence of layers with elevated radiogenic heat productions within the crust can significantly affect its thermal structure and provoke heating during subsidence (Sandiford *et al.*, 1998). Therefore, we infer that the pre-rifting crust structure and composition (inherited from its late Neoproterozoic evolution) played an important role in enhancing melt production at Furongian–Lower Ordovician times.

6 Conclusion

Field relationships, petrography and whole-rock geochemistry collectively indicate that the Cézarenque–Joyeuse gneisses represent former volcanic rocks of rhyodacite composition and their erosion products, originally interlayered within detrital sedimentary sequences. Zircon U–Pb dating of the gneisses demonstrate that the felsic magmas erupted or were emplaced at very shallow crustal levels between 486.1 ± 5.5 Ma and 483.0 ± 5.5 Ma. In that regard, the Cézarenque–Joyeuse gneisses do represent a newly identified

fragment of the Furongian–Lower Ordovician volcanic belt of SW Europe. Inherited zircon date distribution and magmatic zircon trace element systematics further substantiate that the source of the Furongian–Lower Ordovician magmas corresponded to Ediacaran sediments and suggest that the *ferrosilicic* signature they commonly exhibit may be explained by the strongly reduced character of the silicic melts (fO_2 close to the iron–wüstite buffer) acquired through interaction with Lower Cambrian organic matter-bearing sediments (Fig. 13). Such a model would be valid for other Furongian–Lower Ordovician ferrosilicic rocks of the northern Gondwana realm as Lower to Middle Cambrian black shales have been described in the Central Iberian Zone (Álvaro *et al.*, 2020a, b) and in the southern Armorican massif (Pouclet *et al.*, 2017). In light with available paleogeographic constraints, it is inferred that crustal melting took place in an intracontinental rift setting and was enhanced by mantle-derived magma underplating and the anomalously high radiogenic heat production of the Ediacaran sedimentary sequences.

Supplementary Material

Supplementary Table 1. Whole-rock major element compositions of the Cézarenque–Joyeuse gneisses.
Supplementary Table 2. LA–ICP–MS U–Pb isotopic and trace element analyses on zircon – Metadata.
Supplementary Table 3. LA–ICP–MS U–Pb isotopic and trace element analyses of zircon reference materials.
Supplementary Table 4. LA–ICP–MS U–Pb isotopic and trace element analyses of zircon from augen gneiss sample 18CEZ01.
Supplementary Table 5. LA–ICP–MS U–Pb isotopic and trace element analyses of zircon from leucogneiss sample 19CEZ54.
Supplementary Text. Analytical techniques: simultaneous U–Pb dating and trace element analyses in zircon.

The Supplementary Material is available at http://www.bsgf.fr/10.1051/bsgf/2022010/olm.

Acknowledgements. SC warmly thanks Vojtech Janoušek for providing invaluable insights on granitoid petrogenesis and classification schemes. François Faure and Pierre Barbey are thanked for stimulating discussions. The assistance of Laurent Tissandier with the SEM was greatly appreciated. We are grateful to Michel Faure, Jérémie Melleton and Michel Ballèvre for their reviews (and the template of Fig. 1 for the latter) and to Romain Augier and Laurent Jolivet for editorial handling.

References

Álvaro JJ, Bauluz B, Clausen S, Devaere L, Gil Imaz A, Monceret É, *et al.* 2014. Stratigraphic review of the Cambrian-Lower Ordovician volcanosedimentary complexes from the northern Montagne Noire, France. *Stratigraphy* 11: 83–96.

Álvaro JJ, Casas JM, Quesada C. 2020a. Reconstructing the pre-Variscan puzzle of Cambro-Ordovician basement rocks in the south-western European margin of Gondwana. *Geol. Soc. Lond. Spec. Publ.* 503: 531–562.

Álvaro JJ, Sánchez-García T, Puddu C, Casas JM, Díez-Montes A, Liesa M, *et al.* 2020b. Comparative geochemical study on Furongian–earliest Ordovician (Toledanian) and Ordovician (Sardic) felsic magmatic events in south-western Europe: underplating of hot mafic magmas linked to the opening of the Rheic Ocean. *Solid Earth* 11: 2377–2409.

Arnaud F, Boullier AM, Burg JP. 2004. Shear structures and microstructures in micaschists: the Variscan Cévennes duplex (French Massif Central). *J. Struct. Geol.* 26: 855–868.

Ballèvre M, Fourcade S, Capdevila R, Peucat JJ, Cocherie A, Fanning CM. 2012. Geochronology and geochemistry of Ordovician felsic volcanism in the Southern Armorican Massif (Variscan belt, France): Implications for the breakup of Gondwana. *Gondwana Res.* 21: 1019–1036.

Ballèvre M, Martinez Catalan JR, Lopez-Carmona A, Pitra P, Abati J, Fernandez RD, *et al.* 2014. Correlation of the nappe stack in the Ibero-Armorican arc across the Bay of Biscay: a joint French-Spanish project. *Geol. Soc. Lond. Spec. Publ.* 405: 77–113.

Barbarin B. 1999. A review of the relationships between granitoid types, their origins and their geodynamic environments. *Lithos* 46: 605–626.

Barbey P, Villaros A, Marignac C, Montel JM. 2015. Multiphase melting, magma emplacement and P-T-time path in late-collisional context: the Velay example (Massif Central, France). *Bull. Soc. Geol. Fr.* 186: 93–116.

Bea F, Montero P, Zinger T. 2003. The nature, origin, and thermal influence of the granite source layer of Central Iberia. *J. Geol.* 111: 579–595.

Bea F, Montero P, Gonzalez-Lodeiro F, Talavera C. 2007. Zircon inheritance reveals exceptionally fast crustal magma generation processes in Central Iberia during the Cambro-Ordovician. *J. Petrol.* 48: 2327–2339.

Bodinier JL, Burg J-P, Leyreloup AF, Vidal H. 1988. Reliques d'un bassin d'arrière-arc subducté, puis obducté dans la région de Marvejols (Massif central). *Bull. Soc. Geol. Fr.* 4: 21–33

Bonin B, Janoušek V, Moyen J-F. 2020. Chemical variation, modal composition and classification of granitoids. *Geol. Soc. Lond. Spec. Publ.* 491: 9–51.

Bouilhol P, Leyreloup AF, Delor C, Vauchez A, Monié P. 2006. Relationships between lower and upper crust tectonic during doming: the mylonitic southern edge of the Velay metamorphic core complex (Cévennes-French Massif Central). *Geodin. Acta* 19: 137–153

Bouton P, Branger P. 2008. Notice explicative, Carte géol. France (1/50 000), feuille Coulonges-sur-l'Autize (587). BRGM, Orléans.

Boynton WV. Cosmochemistry of the rare earth elements: meteorite studies. In: Henderson P, ed. *Rare Earth Element Geochemistry.* Amsterdam: Elsevier, 1984, pp. 63–114.

Briand B, Bouchardon J-L, Santallier D, Piboule M, Ouali H, Capiez P. 1992. Alkaline affinity of the metabasites in the gneissic series surrounding the Velay migmatitic domain. *Geol. Fr.* 2: 9–15.

Briand B, Bouchardon J-L, Capiez P, Piboule M. 2002. Felsic (A-type)-basic (plume-induced) Early Palaeozoic bimodal magmatism in the Maures Massif (southeastern France). *Geol. Mag.* 139: 291–311.

Brichau S, Respaut J-P, Monié P. 2007. New age constraints on emplacement of the Cévenol granitoids, South French Massif Central. *Int. J. Earth Sci.* 97: 725–738.

Brouder P. 1963. Description d'une succession lithologique avec niveaux-repères dans les schistes cristallins des Cévennes près de Villefort (Lozère). *Bull. Soc. Geol. Fr.* 7: 828–834

Bryan SE. Environmental impact of silicic magmatism in Large Igneous Province events. In: Ernst ER, Dickson AJ, Bekker A, eds.

Large Igneous Provinces: A Driver of Global Environmental and Biotic Changes. American Geophysical Union, 2021, pp. 133–151.
Burnham AD, Berry AJ. 2017. Formation of Hadean granites by melting of igneous crust. *Nat. Geosci.* 10: 457–461.
Burg J-P, Matte P. 1978. A cross section through the French Massif Central and the scope of its Variscan geodynamic evolution. *Z. dt. geol. Ges.* 129: 429–460.
Carignan J, Hild P, Mevelle G, Morel J, Yeghicheyan D. 2001. Routine analyses of trace elements in geological samples using flow Injection and low pressure on-line liquid chromatography coupled to ICP-MS: a study of geochemical reference materials BR, DR-N, UB-N, AN-G and GH. *Geostand. Newsl.* 25: 187–198.
Caron C. 1994. Les minéralisations Pb-Zn associées au Paléozoique inférieur d'Europe méridionale. Traçage isotopique Pb-Pb des gites de l'Iglesiente (SW Sardaigne) et des Cévennes et évolution du socle encaissant par la géochronologie U–Pb, ^{40}Ar–^{39}Ar et K–Ar. Université de Montpellier.
Castro A, García-Casco A, Fernández C, Corretgé LG, Moreno-Ventas I, Gerya T, *et al.* 2009. Ordovician ferrosilicic magmas: Experimental evidence for ultrahigh temperatures affecting a metagreywacke source. *Gondwana Res.* 16: 622–632.
Chantraine J, Autran A, Cavelier C. 2003. Carte géologique de la France à l'échelle du millionième, 6^{e} édition révisée. BRGM, Orléans.
Chelle-Michou C, Laurent O, Moyen J-F, Block S, Paquette JL, Couzinié S, *et al.* 2017. Pre-Cadomian to late-Variscan odyssey of the eastern Massif Central, France: Formation of the West European crust in a nutshell. *Gondwana Res.* 46: 170–190.
Chenevoy M. 1968a. Les gneiss amygdalaires du Massif Central français : anciens tufs ou laves de chimisme rhyodacitique. *C. R. Acad. Sci. Paris* 266: 1921–1923.
Chenevoy M. 1968b. Les gneiss amygdalaires du Massif Central français. *Rev. Geogr. Phys. Geol.* 2: 177–195.
Chenevoy M, Ravier J. 1968. Extension des séries cristallophylliennes à andalousite-cordiérite et à disthène-staurotide dans les Cévennes septentrionales et médianes. *Bull. Soc. Geol. Fr.* 7: 613–617.
Cohen K, Finney S, Gibbard P, Fan J. 2013. The ICS International Chronostratigraphic Chart. *Episodes* 36: 199–204.
Costa S. 1989. Age radiométrique ^{39}Ar–^{40}Ar du métamorphisme des séries du Lot et du charriage du groupe leptyno-amphibolique de Marvejols (M.C.F.). *C. R. Acad. Sci. Paris* 309: 561–567.
Couzinié S. 2017. Evolution of the continental crust and significance of the zircon record, a case study from the French Massif Central. Université de Saint-Étienne.
Couzinié S, Moyen JF, Villaros A, Paquette JL, Scarrow JH, Marignac C. 2014. Temporal relationships between Mg-K mafic magmatism and catastrophic melting of the Variscan crust in the southern part of Velay Complex (Massif Central, France). *J. Geosci.* 59: 69–86.
Couzinié S, Laurent O, Poujol M, Mintrone M, Chelle-Michou C, Moyen JF, *et al.* 2017. Cadomian S-type granites as basement rocks of the Variscan belt (Massif Central, France): Implications for the crustal evolution of the north Gondwana margin. *Lithos* 286-287: 16–34.
Couzinié S, Laurent O, Chelle-Michou C, Bouilhol P, Paquette JL, Gannoun AM, *et al.* 2019. Detrital zircon U–Pb–Hf systematics of Ediacaran metasediments from the French Massif Central: Consequences for the crustal evolution of the north Gondwana margin. *Precambrian Res.* 324: 269–284.
Couzinié S, Bouilhol P, Laurent O, Marko L, Moyen JF. 2021. When zircon drowns: Elusive geochronological record of water-fluxed orthogneiss melting in the Velay dome (Massif Central, France). *Lithos* 384-385: 105938.
Crevola G, Boucarut M, Magontier J, Collomb P. 1983. Origine granitique des gneiss de la Cézarenque (Cévennes, Massif Central) : identification de plusieurs faciès plutoniques originels. *C. R. Acad. Sci. Paris* 296: 1519–1522.
Cuney M, Friedrich M. 1987. Physicochemical and crystal-chemical controls on accessory mineral paragenesis in granitoids: implications for uranium metallogenesis. *Bull. Miner.* 110: 235–247.
Davoine P. 1969. La distinction géochimique ortho-para des leptynites. *Bull. Soc. Fr. Miner. Cr.* 92: 59–75.
de La Roche FH. 1968. Comportement géochimique différentiel de Na, K et Al dans les formations volcaniques et sédimentaires : un guide pour l'étude des formations métamorphiques et plutoniques. *C. R. Acad. Sci. Paris* 267: 39–42.
Debon F, Le Fort P. 1988. A cationic classification of common plutonic rocks and their magmatic associations: principles, method, applications. *Bull. Miner.* 111: 493–510.
Demange M. 1982. Étude géologique du massif de l'Agout (Montagne Noire, France). Université Paris VI.
Dias Da Silva I, Valverde-Vaquero P, Gonzalez-Clavijo E, Diez-Montes A, Martinez Catalan JR. 2014. Structural and stratigraphical significance of U–Pb ages from the Mora and Saldanha volcanic complexes (NE Portugal, Iberian Variscides). *Geol. Soc. Lond. Spec. Publ.* 405: 115–135.
Díaz-Alvarado J, Fernández C, Chichorro M, Castro A, Pereira MF. 2016. Tracing the Cambro–Ordovician ferrosilicic to calc-alkaline magmatic association in Iberia by in situ U–Pb SHRIMP zircon geochronology (Gredos massif, Spanish Central System batholith). *Tectonophysics* 681: 95–110.
Díez Fernández R, Castiñeiras P, Gómez Barreiro J. 2012. Age constraints on Lower Paleozoic convection system: Magmatic events in the NW Iberian Gondwana margin. *Gondwana Res.* 21: 1066–1079.
Díez Montes AD, Catalán JRM, Mulas FB. 2010. Role of the Ollo de Sapo massive felsic volcanism of NW Iberia in the Early Ordovician dynamics of northern Gondwana. *Gondwana Res.* 17: 363–376.
Diot H, Féménias O, Moreau C, Gaufriau A, Roy CL, Karnay G. 2007. Notice explicative, Carte géol. France (1/50 000), feuille Fontenay-le-Comte (586). BRGM, Orléans.
El Korh A, Schmidt ST, Ballèvre M, Ulianov A, Bruguier O. 2012. Discovery of an albite gneiss from the Île de Groix (Armorican Massif, France): geochemistry and LA–CP–MS U–Pb geochronology of its Ordovician protolith. *Int. J. Earth Sci.* 101: 1169–1190.
Elmi S, Feys R, Samama JC, Weisbrod A. 1974. Notice explicative, Carte géol. France (1/50 000), feuille Largentière (864). BRGM, Orléans.
Elmi S, Brouder P, Berger G, Gras H, Busnardo R, Bérard P, *et al.* 1989. Notice explicative, Carte géol. France (1/50 000), feuille Bessèges (888). BRGM, Orléans.
Farias P, Casado BO, Marcos A, Rubio-Ordoñez A, Fanning CM. 2014. U–Pb zircon SHRIMP evidences of Cambrian volcanism in the Schistose Domain within the Galicia-Tras-os-Montes Zone (Variscan Orogen, NW Iberian Peninsula). *Geol. Acta* 12: 209–218.
Faure M, Charonnat X, Chauvet A, Chen Y, Talbot JY, Martelet G. 2001. Tectonic evolution of the Cévennes para-autochthonous domain of the Hercynian French Massif Central and its bearing on ore deposits formation. *Bull. Soc. Geol. Fr.* 172: 687–696.
Faure M, Brouder P, Thierry J, Alabouvette B, Cocherie A, Bouchot V. 2009a. Notice explicative, Carte géol. France (1/50 000), feuille Saint-André-de-Valborgne (911). BRGM, Orléans.

Faure M, Lardeaux J-M, Ledru P. 2009b. A review of the pre-Permian geology of the Variscan French Massif Central. *C. R. Geosci.* 341: 202–213.

Fernández C, Becchio R, Castro A, Viramonte JM, Moreno-Ventas I, Corretgé LG. 2008. Massive generation of atypical ferrosilicic magmas along the Gondwana active margin: Implications for cold plumes and back-arc magma generation. *Gondwana Res.* 14: 451–473.

Ferry JM, Watson EB. 2007. New thermodynamic models and revised calibrations for the Ti-in-zircon and Zr-in-rutile thermometers. *Contrib. Miner. Petrol.* 154: 429–437.

Fiannacca P, Williams IS, Cirrincione R, Pezzino A. 2019. Polyorogenic melting of metasedimentary crust from a granite geochemistry and inherited zircon perspective (Southern Calabria-Peloritani Orogen, Italy). *Front. Earth Sci.* 7.

Frost BR, Barnes CG, Collins WJ, Arculus RJ, Ellis DJ, Frost CD. 2001. A geochemical classification for granitic rocks. *J. Petrol.* 42: 2033–2048.

Gaillard F, Scaillet B, Pichavant M, Bény J-M. 2001. The effect of water and fO_2 on the ferric-ferrous ratio of silicic melts. *Chem. Geol.* 174: 255–273.

Galbraith RF. 2005. Statistics for fission track analysis. CRC Press.

Gao P, Zheng Y-F, Zhao Z-F. 2016. Distinction between S-type and peraluminous I-type granites: Zircon versus whole-rock geochemistry. *Lithos* 258-259: 77–91.

García-Arias M, Díez Montes A, Villaseca C, Blanco-Quintero IF. 2018. The Cambro-Ordovician Ollo de Sapo magmatism in the Iberian Massif and its Variscan evolution: A review. *Earth-Sci. Rev.* 176: 345–372.

Garfunkel Z. 2015. The relations between Gondwana and the adjacent peripheral Cadomian domain – Constrains on the origin, history, and paleogeography of the peripheral domain. *Gondwana Res.* 28: 1257–1281.

Gieré R. 1996. Formation of rare earth minerals in hydrothermal systems. In: Jones AP, Wall F, Williams CT, eds. *Rare Earth Minerals: Chemistry, Origin and Ore Deposits*. London, UK: Chapman and Hall, pp. 105–150.

Guérangé-Lozes J, Burg J-P. 1990. Variscan nappes in the southwest of the Massif Central (1:250 000 geological and structural maps of Montpellier and Aurillac). *Geol. Fr.* 3-4: 71–106.

Gutiérrez-Alonso G, Gutiérrez-Marco JC, Fernández-Suárez J, Bernárdez E, Corfu F. 2016. Was there a super-eruption on the Gondwanan coast 477 Ma ago? *Tectonophysics* 681: 85–94.

Harlaux M. 2016. Les systèmes métallogéniques hydrothermaux à tungstène et métaux rares (Nb, Ta, Sn) dans le contexte orogénique fini-varisque : exemple du Massif Central Français. Université de Lorraine.

Holtz F, Johannes W. 1994. Maximum and minimum water contents of granitic melts: implications for chemical and physical properties of ascending magmas. *Lithos* 32: 149–159.

Holtz F, Johannes W, Pichavant M. 1992. Peraluminous granites: the effect of alumina on melt composition and coexisting minerals. *Earth Environ. Sci. Trans. R. Soc. Edinb.* 83: 409–416.

Horstwood MSA, Košler J, Gehrels G, Jackson SE, McLean NM, Paton C, *et al.* 2016. Community-Derived Standards for LA–ICP–MS U–(Th–)Pb Geochronology – Uncertainty propagation, age interpretation and data reporting. *Geostand. Geoanal. Res.* 40: 311–332.

Iacono-Marziano G, Gaillard F, Scaillet B, Polozov A, Marecal V, Pirre M, *et al.* 2012. Extremely reducing conditions reached during basaltic intrusion in organic matter-bearing sediments. *Earth Planet. Sci. Lett.* 357-358: 319–326.

Ishihara S. 2004. The redox state of granitoids relative to tectonic setting and earth history: The magnetite-ilmenite series 30 years later. *Earth Environ. Sci. Trans. R. Soc. Edinb.* 95: 23–33.

Janoušek V, Farrow CM, Erban V. 2006. Interpretation of whole-rock geochemical data in igneous geochemistry: introducing GeoChemical Data toolkit (GCDkit). *J. Petrol.* 47: 1255–1259.

Kroner U, Romer RL. 2013. Two plates – Many subduction zones: The Variscan orogeny reconsidered. *Gondwana Res.* 24: 298–329.

Lacassin R, van den Driessche FJ. 1983. Finite strain determination of gneiss: Application of Fry's method to porphyroid in the southern Massif Central (France). *J. Struct. Geol.* 5: 245–253.

Laurent O, Couzinié S, Zeh A, Vanderhaeghe O, Moyen JF, Villaros A, *et al.* 2017. Protracted, coeval crust and mantle melting during Variscan late-orogenic evolution: U–Pb dating in the eastern French Massif Central. *Int. J. Earth Sci.* 106: 421–451.

Le Bas MJL, Le Maitre RW, Streckeisen A, Zanettin B. 1986. A chemical classification of volcanic rocks based on the total alkali-silica diagram. *J. Petrol.* 27: 745–750.

Ledru P, Lardeaux JM, Santallier D, Autran A, Quenardel JM, Floc'h JP, *et al.* 1989. Where are the nappes in the French Massif central? *Bull. Soc. Geol. Fr.* 8: 605–618.

Ledru P, Courrioux G, Dallain C, Lardeaux JM, Montel JM, Vanderhaeghe O, *et al.* 2001. The Velay dome (French Massif Central): melt generation and granite emplacement during orogenic evolution. *Tectonophysics* 342: 207–237

Loader MA, Wilkinson JJ, Armstrong RN. 2017. The effect of titanite crystallisation on Eu and Ce anomalies in zircon and its implications for the assessment of porphyry Cu deposit fertility. *Earth Planet. Sci. Lett.* 472: 107–119.

Lopez-Sanchez MA, Iriondo A, Marcos A, Martínez FJ. 2015. A U–Pb zircon age (479 ± 5 Ma) from the uppermost layers of the Ollo de Sapo Formation near Viveiro (NW Spain): implications for the duration of rifting-related Cambro–Ordovician volcanism in Iberia. *Geol. Mag.* 152: 341–350.

Lotout C, Pitra P, Poujol M, Anczkiewicz R, Van Den Driessche J. 2018. Timing and duration of Variscan high-pressure metamorphism in the French Massif Central: A multimethod geochronological study from the Najac Massif. *Lithos* 308-309: 381–394.

Lotout C, Poujol M, Pitra P, Anczkiewicz R, Van Den Driessche J. 2020. From burial to exhumation: Emplacement and metamorphism of mafic eclogitic terranes constrained through multimethod petrochronology, case study from the Lévézou Massif (French Massif Central, Variscan Belt). *J. Petrol.* 61.

Magontier J. 1988. Étude géologique de la Gardonenque entre St-Jean-du-Gard et la Grand'Combe à l'ouest d'Alès, Gard-France. Université Bordeaux 3.

Mattauer M, Etchecopar A. 1976. Arguments en faveur de chevauchements du type himalayen dans la chaine hercynienne du Massif Central français. *Coll. Int. CNRS* 268: 261–267.

Matte P. Variscan thrust nappes, detachments, and strike-slip faults in the French Massif Central: Interpretation of the lineations. In: Hatcher Jr RD, Carlson MP, McBride JH, Martínez Catalán JR, eds. *4-D Framework of Continental Crust*. Geological Society of America, 2007, pp. 391–402.

Matzel JEP, Bowring SA, Miller RB. 2006. Time scales of pluton construction at differing crustal levels: Examples from the Mount Stuart and Tenpeak intrusions, North Cascades, Washington. *GSA Bull.* 118: 1412–1430.

Melleton J, Cocherie A, Faure M, Rossi P. 2010. Precambrian protoliths and Early Paleozoic magmatism in the French Massif Central: U–Pb data and the North Gondwana connection in the west European Variscan belt. *Gondwana Res.* 17: 13–25.

Montel JM, Marignac C, Barbey P, Pichavant M. 1992. Thermobarometry and granite genesis: the Hercynian low-P, high-T Velay anatectic dome (French Massif Central). *J. Metamorph. Geol.* 10: 1–15.

Montel JM, Foret S, Veschambre M, Nicollet C, Provost A. 1996. Electron microprobe dating of monazite. *Chem. Geol.* 131: 37–53.

Montero P, Bea F, González-Lodeiro F, Talavera C, Whitehouse MJ. 2007. Zircon ages of the metavolcanic rocks and metagranites of the Ollo de Sapo Domain in central Spain: implications for the Neoproterozoic to Early Palaeozoic evolution of Iberia. *Geol. Mag.* 144: 963–976.

Montero P, Talavera C, Bea F, Lodeiro FG, Whitehouse MJ. 2009. Zircon geochronology of the Ollo de Sapo Formation and the age of the Cambro–Ordovician rifting in Iberia. *J. Geol.* 117: 174–191.

Montero P, Talavera C, Bea F. 2017. Geochemical, isotopic, and zircon (U–Pb, O, Hf isotopes) evidence for the magmatic sources of the volcano-plutonic Ollo de Sapo Formation, Central Iberia. *Geol. Acta* 15: 245–260.

Moyen JF, Laurent O, Chelle-Michou C, Couzinié S, Vanderhaeghe O, Zeh A, *et al.* 2017. Collision vs. subduction-related magmatism: Two contrasting ways of granite formation and implications for crustal growth. *Lithos* 277: 154–177.

Murphy JB, Gutiérrez-Alonso G, Fernández-Suárez J, Braid JA. 2008. Probing crustal and mantle lithosphere origin through Ordovician volcanic rocks along the Iberian passive margin of Gondwana. *Tectonophysics* 461: 166–180.

Nance RD, Gutiérrez-Alonso G, Keppie JD, Linnemann U, Murphy JB, Quesada C, *et al.* 2010. Evolution of the Rheic Ocean. *Gondwana Res.* 17: 194–222.

Ni Z, Arevalo R, Piccoli P, Reno BL. 2020. A novel approach to identifying mantle-equilibrated zircon by using trace element chemistry. *Geochem. Geophys. Geosyst.* 21.

Oggiano G, Gaggero L, Funedda A, Buzzi L, Tiepolo M. 2010. Multiple early Paleozoic volcanic events at the northern Gondwana margin: U–Pb age evidence from the Southern Variscan branch (Sardinia, Italy). *Gondwana Res.* 17: 44–58.

Oriolo S, Schulz B, Geuna S, González PD, Otamendi JE, Sláma J, *et al.* 2021. Early Paleozoic accretionary orogens along the Western Gondwana margin. *Geosci. Front.* 12: 109–130.

Parga Pondal I, Matte P, Capdevila R. 1964. Introduction à la géologie de l'« Ollo de Sapo », formation porphyroide anté-silurienne du Nord-Ouest de l'Espagne. *Notas. Comun. Inst. Geol. Min. Esp.* 76: 119–153.

Pin C, Marini F. 1993. Early Ordovician continental break-up in Variscan Europe: Nd–Sr isotope and trace element evidence from bimodal igneous associations of the Southern Massif Central, France. *Lithos* 29: 177–196.

Pouclet A, Álvaro JJ, Bardintzeff J-M, Imaz AG, Monceret E, Vizcaïno D. 2017. Cambrian–early Ordovician volcanism across the South Armorican and Occitan domains of the Variscan Belt in France: Continental break-up and rifting of the northern Gondwana margin. *Geosci. Front.* 8: 25–64.

Quesnel F, Prost AE, Lablanche G, Thiry M, Simon-Coinçon R, Théveniaut H, *et al.* 2009. Notice explicative, Carte géol. France (1/50 000), feuille Châteaumeillant (595). BRGM, Orléans.

Rakib A. 1996. Le métamorphisme régional de basse pression des Cévennes occidentales : une conséquence directe de la mise en place du dôme thermique vellave (Massif central français). Université de Montpellier.

Rittman A. 1957. On the serial character of igneous rocks. *Egypt J. Geol.* 1: 23–48.

Roger G. 1969. Étude géologique de la Cézarenque et du SE du Mont Lozère. *Mémoires du BRGM (Paris)* 66.

Rudnick RL, Gao S. 2003. Composition of the continental crust. In: Rudnick RL, ed. *The Crust*. Oxford: Elsevier-Pergamon, pp. 1–64.

Sandiford M, Hand M, McLaren S. 1998. High geothermal gradient metamorphism during thermal subsidence. *Earth Planet. Sci. Lett.* 163: 149–165.

Schiller D, Finger F. 2019. Application of Ti-in-zircon thermometry to granite studies: problems and possible solutions. *Contrib. Miner. Petrol.* 174: 51.

Seyler M. 1986. Petrology and genesis of hercynian alkaline orthogneisses from Provence, France. *J. Pet.* 27: 1229–1251.

Spencer CJ, Kirkland CL, Taylor RJM. 2016. Strategies towards statistically robust interpretations of in situ U–Pb zircon geochronology. *Geosci. Front.* 7: 581–589.

Stevens G, Villaros A, Moyen J-F. 2007. Selective peritectic garnet entrainment as the origin of geochemical diversity in S-type granites. *Geology* 35: 9–12.

Talavera C, Montero P, Bea F, González Lodeiro F, Whitehouse M. 2013. U–Pb Zircon geochronology of the Cambro–Ordovician metagranites and metavolcanic rocks of central and NW Iberia. *Int. J. Earth Sci.* 102: 1–23.

Tobschall HJ. 1971. Zur genese der migmatite des Beaume-Tales (Mittlere Cévennen, Dép. Ardèche). *Contrib. Miner. Petrol.* 32: 93–111.

Toteu SF, Macaudière J. 1984. Complex synkinematic and postkinematic garnet porphyroblast growth in polymetamorphic rocks. *J. Struct. Geol.* 6: 669–677.

Trail D, Bruce Watson E, Tailby ND. 2012. Ce and Eu anomalies in zircon as proxies for the oxidation state of magmas. *Geochim. Cosmochim. Acta* 97: 70–87.

Valverde-Vaquero P, Marcos A, Farias P, Gallastegui G. 2005. U–Pb dating of Ordovician felsic volcanism in the Schistose Domain of the Galicia-Trás-os-Montes Zone near Cabo Ortegal (NW Spain). *Geol. Acta* 3: 27–38.

Vanderhaeghe O, Laurent O, Gardien V, Moyen JF, Gébelin A, Chelle-Michou C, *et al.* 2020. Flow of partially molten crust controlling construction, growth and collapse of the Variscan orogenic belt: the geologic record of the French Massif Central. *BSGF – Earth Sci. Bull.* 191: 25.

Venables WN, Ripley BD. 2002. Modern applied statistics with S, 4th ed. Springer.

Vermeesch P. 2021. Maximum depositional age estimation revisited. *Geosci. Front.* 12: 843–850.

Villaros A, Laurent O, Couzinié S, Moyen JF, Mintrone M. 2018. Plutons and domes: the consequences of anatectic magma extraction – Example from the southeastern French Massif Central. *Int. J. Earth Sci.* 107: 2819–2842.

Villaseca C, Barbero L, Herreros V. 1998. A re-examination of the typology of peraluminous granite types in intracontinental orogenic belts. *Earth Environ. Sci. Trans. R. Soc. Edinb.* 89: 113–119.

Villaseca C, Merino Martínez E, Orejana D, Andersen T, Belousova E. 2016. Zircon Hf signatures from granitic orthogneisses of the Spanish Central System: Significance and sources of the Cambro–Ordovician magmatism in the Iberian Variscan Belt. *Gondwana Res.* 34: 60–83.

von Raumer JF, Stampfli GM, 2018. Ollo de Sapo Cambro–Ordovician volcanics from the Central Iberian basement – A multiphase evolution. *Terra Nova* 30: 350–358.

Wang Q, Zhu D-C, Zhao Z-D, Guan Q, Zhang XQ, Sui QL, *et al.* 2012. Magmatic zircons from I-, S- and A-type granitoids in Tibet: Trace element characteristics and their application to detrital zircon provenance study. *J. Asian Earth Sci.* 53: 59–66.

Watson EB. 1996. Dissolution, growth and survival of zircons during crustal fusion: kinetic principals, geological models and implications for isotopic inheritance. *Earth Environ. Sci. Trans. R. Soc. Edinb.* 87: 43–56.

Watson EB, Harrison TM. 1983. Zircon saturation revisited: temperature and composition effects in a variety of crustal magma types. *Earth Planet. Sci. Lett.* 64: 295–304.

Weisbrod A. 1968. Les conditions du métamorphisme dans les Cévennes médianes (Massif Central, France). *C. R. Acad. Sci. Paris* 266: 755–757.

Weisbrod A. 1969. Caractères géochimiques et origine des « schistes amygdalaires » des Cévennes (Massif Central français). *C. R. Acad. Sci. Paris* 268: 3018–3020.

Weisbrod A. 1970. Pétrologie du socle métamorphique des Cévennes médianes (Massif Central français) : reconstitution sédimentologique et approche thermodynamique du métamorphisme. Université de Nancy.

Weisbrod A, Marignac C. 1968. Sur l'origine des « schistes amygdalaires » des Cévennes (Massif Central français). *C. R. Acad. Sci. Paris* 266: 865–867.

Whalen JB, Chappell BW. 1988. Opaque mineralogy and mafic mineral chemistry of I- and S-type granites of the Lachlan fold belt, Southeast Australia. *Am. Miner.* 73: 281–296.

Wilke S, Holtz F, Neave DA, Almeev R. 2017. The effect of anorthite content and water on quartz-feldspar cotectic compositions in the rhyolitic system and implications for geobarometry. *J. Petrol.* 58: 789–818.

Cite this article as: Couzinié S, Bouilhol P, Laurent O, Grocolas T, Montel J-M. 2022. Cambro–Ordovician ferrosilicic magmatism along the northern Gondwana margin: constraints from the Cézarenque–Joyeuse gneiss complex (French Massif Central), *BSGF - Earth Sciences Bulletin* 193: 15.